Mechanical Characterization of Carbon Fiber and Thermoplastic Ankle Foot Orthoses

Amanda Wach
Marquette University

MECHANICAL CHARACTERIZATION OF CARBON FIBER AND THERMOPLASTIC ANKLE FOOT ORTHOSES

by

Amanda M. Wach, B.S.

A Thesis submitted to the Faculty of the Graduate School,
Marquette University,
in Partial Fulfillment of the Requirements for
the Degree of Master of Science

Milwaukee, Wisconsin

December 2015

ABSTRACT
MECHANICAL CHARACTERIZATION OF CARBON FIBER AND THERMOPLASTIC ANKLE FOOT ORTHOSES

Amanda M. Wach, B.S.

Marquette University, 2015

The needs of an increasingly young and active orthotic patient population has led to advancements in ankle foot orthosis (AFO) design and materials to enable higher function. The Intrepid Dynamic Exoskeletal Orthosis (IDEO) is a custom energy-storing carbon fiber AFO that has demonstrated improved clinical function, allowing patients to return to high-intensity activities such as sports and military service. An improved understanding of AFO mechanical function will aid prescription and fitting, as well as assist in design modifications for different patient populations. This study investigated the mechanical properties of AFOs, specifically structural stiffness, rotational motion, and strut deflection, to discern design characteristics contributing to increased functional outcomes.

Seven AFOs of different designs and materials were tested under cyclical loading to characterize their mechanical properties. These AFOs were fitted about a surrogate limb and underwent pseudo-static compressive testing using a materials testing system and motion analysis. Acquired data included: compressive force, vertical displacement, kinematic data, and ankle rotation. Testing was conducted at discrete orientations and loads corresponding to the latter sub-phases of stance: midstance, terminal stance, and pre-swing. The compressive stiffness, posterior strut deflection, and rotational motion of the various AFOs, as well as the ankle range of motion (ROM) of the surrogate limb, were characterized.

The deformation of the various AFO designs during loading differed greatly, influencing the observed mechanical behavior. Traditional thermoplastic and carbon fiber designs deformed at the malleolar flares or rotationally at the ankle, demonstrating low proximal rotational motion of the AFO and large surrogate ankle ROM. The mechanical response of the IDEO was unique, with large deflection observed along the posterior strut, minimal footplate deformation, greater proximal rotational motion, and minimal ankle ROM. This design incorporates stiffer materials for fabrication, increasing the potential for energy storage, while restricting ankle motion. Enhanced knowledge of the mechanical behavior and energy storage/release mechanism may improve prescription, custom design and fitting of the IDEO.

ACKNOWLEDGMENTS

Amanda M. Wach, B.S.

First and foremost, I would like to thank my advisor, Dr. Silver-Thorn. Thank you for all of your help and guidance each step of the way, from inception to my final draft, and for pushing me towards great opportunities.

Thank you, Dr. Wang and Ms. McGrady, for your assistance in my testing design and data collection. Without you I would have over complicated every aspect of my testing, and would have never finished collecting data. Thank you for your help and patience.

I would also like to thank my committee members: Dr. Jeutter, for your patience and assistance with the inductive sensor; Dr. Voglewede, for your insight on how to demonstrate the mechanical behavior of the IDEO design; and Dr. Harris, for challenging me to bring my work into the context of a bigger picture.

To Tom Current, thank you for conceiving this project, including me, and making this all happen! Thank you for all of your work in fabricating orthoses and connecting me with Hanger Prosthetics & Orthotics.

I thank my support group of family and friends, especially Jeff, CarrieAnn, Sarah, and Samantha, for your encouragement. To Jimmy, my rock, I would not have made it this far without your unwavering confidence in me.

Finally, I would like to acknowledge the Department of Biomedical Engineering at Marquette University for the financial support and Hanger Prosthetics & Orthotics for providing the orthoses and prosthetic components used in this study, and for additional financial support.

TABLE OF CONTENTS

LIST OF TABLES

LIST OF FIGURES

CHAPTER 1: INTRODUCTION

Ankle-foot orthoses (AFOs) are devices used to control and stabilize the lower leg to improve pathological gait [1, 2] due to muscle weakness, spasticity, hypertonicity, instability, and/or chronic pain [1]. In addition to post-stroke individuals, AFOs have been prescribed for young, formerly-active individuals with traumatic injuries to the lower leg and ankle-foot complex, resulting in irreversible damage to the physical structure, along with chronic pain [1]. Recent advancements in surgical techniques offer limb salvage as an alternative treatment option to amputation for traumatic injury, resulting in an atypical AFO patient population [3, 4]. These individuals, including military personnel as well as other formerly-active patients who have suffered lower extremity trauma, desire to return to high-intensity activities beyond simple walking and demand higher levels of function from their orthotic devices.

For the past fifty years, AFO designs have traditionally been fabricated from thermoplastic materials to provide function while maintaining light and cosmetically acceptable devices [1]. Thermoplastic AFO designs have been used to stabilize the subtalar and ankle joints, position the foot, and/or assist dorsiflexion during gait [2]. These designs have been shown to improve walking (e.g., increase walking speed, increase step and stride lengths, enhance balance, etc.) [5, 6]. However, tested thermoplastic designs are unable to produce sufficient energy storage and return to facilitate high-intensity activities such as running and jumping [7, 8].

To improve the energy storage and return of AFO designs, carbon fiber composite materials have been used in fabrication. Carbon fiber composites are strong and lightweight and have been used successfully to increase energy storage and return in prosthetic devices (e.g., Flex foot and Cheetah running foot, Otto Bock). Carbon fiber posterior struts can be incorporated into traditional AFO designs, using the strut to link the footplate and proximal cuff [2]. Alternatively, new designs comprised of solely

carbon fiber composite materials can be fabricated, resulting in thinner, lighter, and stronger designs [2]. One innovative device, the Intrepid Dynamic Exoskeletal Orthosis (IDEO), integrates carbon graphite pylon struts with a carbon fiber footplate and proximal cuff. While the IDEO and other carbon fiber AFOs have resulted in improved functional performance in terms of temporal-spatial parameters (e.g., walking speed, cadence, step and stride length) and energy cost [7-12], the dynamic mechanical behavior of these devices is poorly understood.

The mechanical properties of an AFO design influence the biomechanical behavior of the AFO-limb complex during gait. One important mechanical characteristic of an AFO is its rotational stiffness, resisting ankle rotation, often considered in the sagittal plane [13]. Due to the interaction between the AFO and lower limb during gait, specifically during stance phase, rotational stiffness may be used to quantify sagittal plane moment-angle behavior [14]. A similar mechanical characteristic, compressive stiffness, has also been investigated for lower limb orthoses. In contrast to rotational stiffness, compressive stiffness is the resistance to compressive loading or displacement, not rotation. (The term, structural stiffness, includes both rotational and compressive stiffness characterization.) Though this characteristic provides less intuitive insight into the biomechanical behavior of the AFO-limb complex, it supports comparison and classification of different orthotic designs. A final mechanical characteristic relevant to lower limb orthoses is the deflection mechanism, a parameter that has been used contrast energy storage/release mechanisms of prosthetic feet [15]. The deflection mechanism is the observed change in AFO geometry in response to an applied force and can be characterized by measures such as strut deflection and relative rotation of AFO segments. Understanding the mechanical properties of AFOs, specifically rotational stiffness and deflection, during late stance may give insight into the potential energy return contributing to enhanced clinical performances of high energy tasks. Improved understanding of a design's potential functional performance may enhance prescription, fitting and alignment, and ultimately, functional outcomes.

The primary hypothesis motivating this research is the deflection mechanism of AFOs under load will differ between designs. Specifically, the IDEO will demonstrate greater displacement throughout the posterior strut and greater rotational movement of the proximal and distal segments of the orthosis compared to traditional thermoplastic and alternative carbon-fiber designs. The increased strut displacement and atypical deflection mechanism is proposed as a mechanism affecting energy storage during loading, contributing to the improvements in functional performance observed clinically. The objectives of this study are: 1) to quantify force-deflection curves, characterizing the structural stiffness of the IDEO and other AFO designs, 2) to quantify the deflection of the posterior strut, and 3) to characterize the relative rotation of the proximal and distal segments of each AFO. Characterizing the mechanical properties of the AFO designs will aid in prescription and orthotic design refinements to accommodate the biomechanical needs of the individual. These quantitative data may assist the development of theories and mechanical models to further explain the observed clinical functional outcomes of improved designs and may result in greater accessibility of these devices.

CHAPTER 2: BACKGROUND AND LITERATURE REVIEW

This chapter will summarize background literature relevant to the project scope, as well as a literature review regarding the mechanical testing of AFOs. Topics include able-bodied gait, ankle gait deviations, current AFO designs and prescription, and mechanical testing of AFOs.

2.1 Able-bodied Gait

General ambulation is studied and characterized by gait analysis. Analysis of the gait cycle typically uses motion capture systems and force plates or instrumented treadmills to quantify the temporal-spatial parameters, kinematics, and kinetics of gait. Walking gait results from controlled and cyclical motion of the lower body. A detailed description of the foot and ankle during able-bodied gait will assist in understanding the functional objectives of orthotic designs to improve gait.

2.1.1 The Gait Cycle Phases

The gait cycle consists of two phases: stance and swing (Figure 1). Stance phase, when the foot is in contact with the ground, can be further divided into sub-phases: initial contact (IC), loading response (LR), mid stance (MSt), terminal stance (TSt), and pre swing (PSw). The first two phases of stance, IC and LR, absorb shock and stabilize the limb as the lower leg transitions to single limb support. Through MSt and TSt, the body moves forward over and anterior to the ipsilateral foot as the contralateral limb swings forward. During PSw, weight is transferred from the ipsilateral to the contralateral limb in preparation for swing phase. Swing phase is the portion of the gait cycle during which the foot is off the ground and advances forward in preparation for the next step. The leg accelerates from initial swing to midswing, and decelerates during terminal swing to prepare for stance.

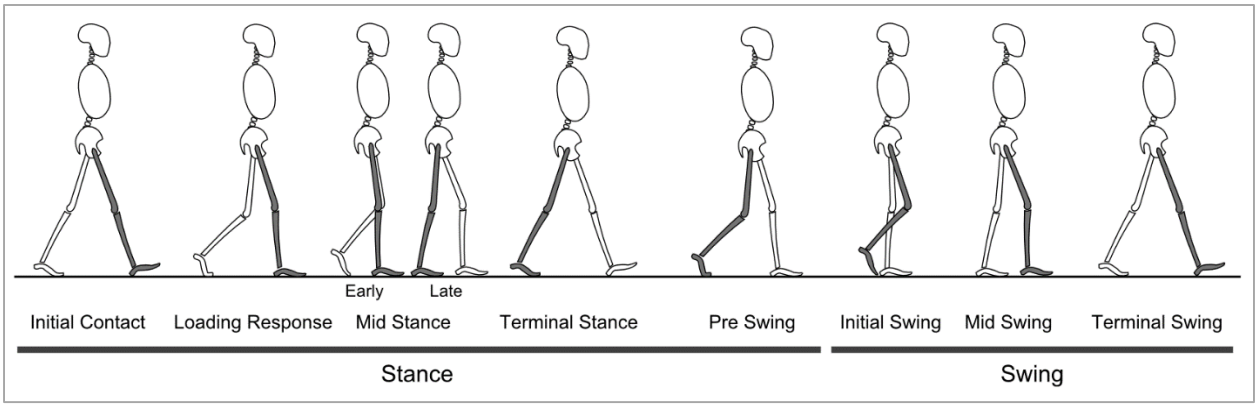

Figure 1: The gait cycle is separated into two phases, stance and swing, with eight sub-phases. Adapted from [16].

2.1.2 Kinematics of the Ankle

Ankle motion during stance is important for forward progression and initial shock absorption [16]. The ankle transitions through different arcs of motion: plantar flexion, dorsiflexion, then plantar flexion, over a 20°-30° range of motion during stance (Figure 2a) [16]. At IC, the ankle is at a neutral angle and quickly plantar flexes to provide stable, full-foot contact with the ground. The tibia then rotates over the foot, dorsiflexing the ankle through MSt. Maximum dorsiflexion, approximately 10°, is reached during TSt, at the end of single limb support. The subsequent double limb support provides stability for rapid ankle plantar flexion to prepare for toe-off at the beginning of swing [16]. During swing, the ankle dorsiflexes to ensure toe clearance as the lower limb advances in preparation for IC.

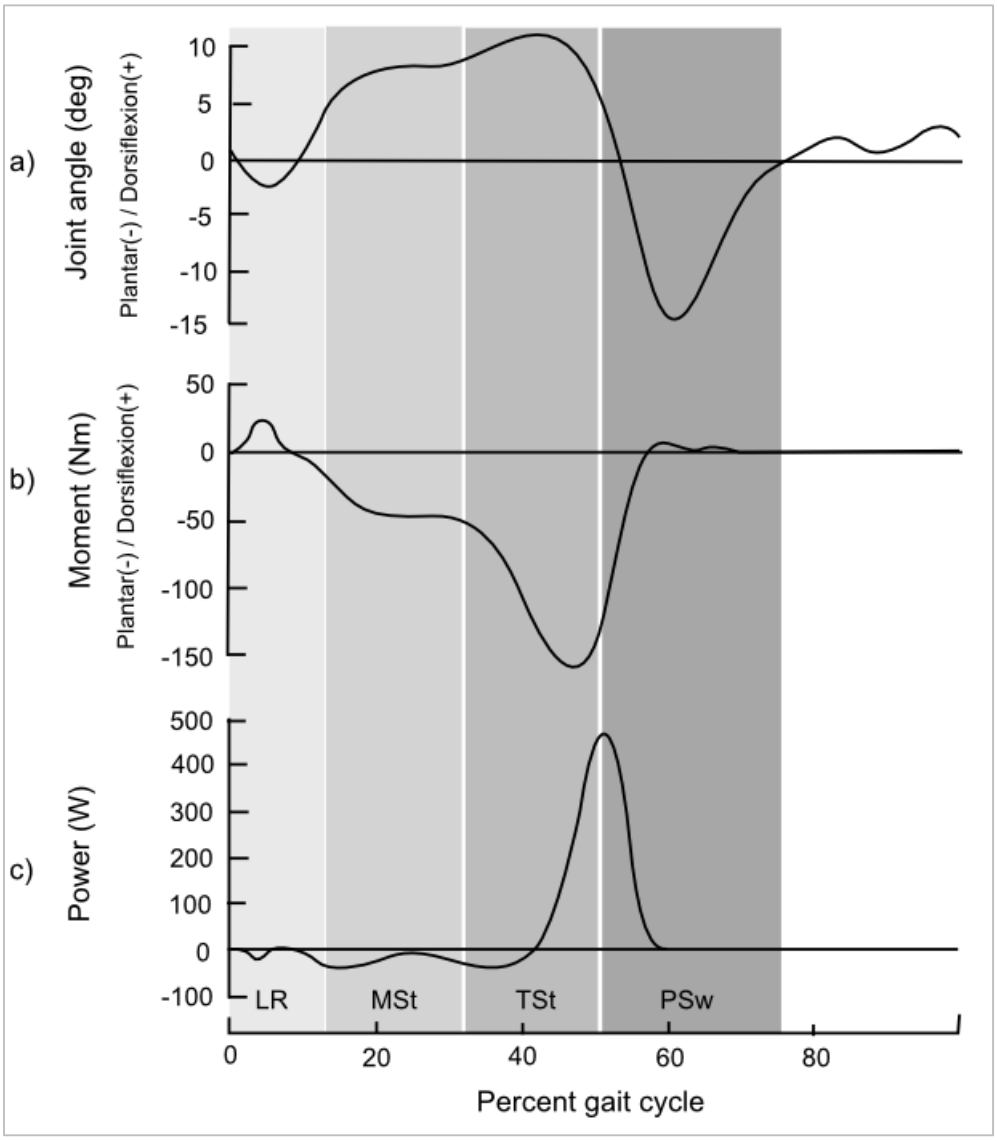

Figure 2: Kinematic and kinetic data of the ankle joint throughout the gait cycle. Sub-phases of stance, excluding IC, are shaded. Adapted from [17].

2.1.3 Rockers of Gait

From LR to TSt, the forward progression of the body over the supporting foot is facilitated by three functional rockers (Figure 3) [16]. These rockers provide a smooth transition through stance, maintaining an extended and stable knee position [16]. The first rocker, the heel rocker, occurs during LR where the foot and lower limb rotate about the heel to achieve foot flat. At the second rocker, the ankle rocker, the lower limb rotates about the ankle; the tibia rotates such that the ankle is dorsiflexed while the

foot maintains full contact with the ground. At TSt, the lower limb and hindfoot rotate over the forefoot about the metatarsal heads, the third rocker, to advance into PSw [16].

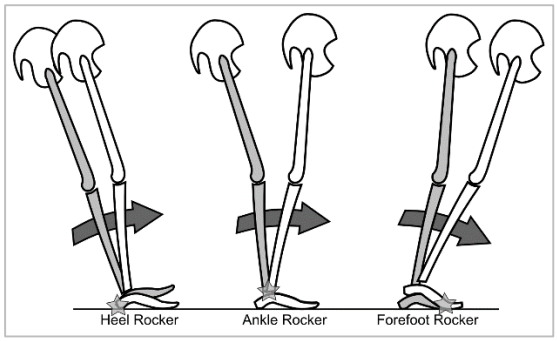

Figure 3: Progression over the three functional rockers. Adapted from [16].

2.1.4 Kinetics of the Ankle

Kinetic moment patterns show forces acting to alter the angular rotation of the ankle during gait (Figure 2b) [17]. During IC and LR, a small dorsiflexor muscle moment controls the ankle plantar flexion, providing a smooth transition to foot flat. During single limb support, from MSt and TSt, a plantar flexor moment stabilizes the lower leg as it rotates about the second ankle rocker. This plantar flexor moment increases, contributing to heel rise, with subsequent rapid ankle plantar flexion [17] and powered push-off to propel the lower leg into swing. The energy generated in this phase results in 80-85% of that generated during the entire gait cycle [17]. As the lower leg transitions into swing, a small dorsiflexor muscle moment occurs to dorsiflex the ankle and aid toe clearance during swing.

2.2 Ankle and Foot Gait Deviations

Lower limb pathologies such as deformity, neurological damage, muscle weakness, muscle spasticity, hypertonicity, instability, and chronic pain can result in abnormal gait. Common gait deviations of the ankle and foot can be classified as excessive plantar flexion, often resulting from insufficient dorsiflexion, or excessive dorsiflexion. As ankle and foot gait deviations are often corrected with the use

of AFOs, an understanding of these deviations and their causes is critical when prescribing an orthotic device.

2.2.1 Excessive Plantar Flexion

Excessive plantar flexion adversely affects tibial progression, resulting in a shortened stride length and reduced walking speed [16]. Depending on the severity and underlying cause of plantar flexion, IC occurs with a low heel or at the forefoot. With low heel contact, IC occurs with the foot nearly parallel to the ground, reducing heel rocker motion in LR [16]. A forefoot strike can lead to three potential LR patterns: heel drop, heel drop with backwards tibial progression, and prolonged heel off [16]. Tibial advancement about the second ankle rocker is severely limited by excessive plantar flexion, contributing to a short step length. Compensatory gait deviations include premature heel rise and knee hyperflexion [16]. In severe cases, the ankle rocker is absent; limb advancement occurs solely through the third rocker. Ankle plantar flexion affects TSt only when additional heel rise is unattainable, hindering roll over the third rocker [16]. While PSw is generally unaffected by excessive plantar flexion, toe clearance during swing phase is greatly reduced leading to compensatory hip and/or knee flexion, circumduction, or vaulting on the stance limb.

Various causes of excessive plantar flexion, such as dorsiflexor weakness, plantar flexor contracture, or soleus and/or gastrocnemius spasticity, result in different gait pathologies. For example, dorsiflexor weakness affects the sub-phases of gait where dorsiflexion is required. At IC and LR, a lack of dorsiflexion results in low heel contact and uncontrolled plantar flexion, or foot slap [16]. The other sub-phases of stance are not affected. The effect of plantar flexion contracture is dependent on the severity of lost dorsiflexion and tissue rigidity [16]. A rigid 30° plantar flexion contraction affects almost all phases of gait, preventing heel contact throughout stance. As a result, the forefoot is the only support structure and stride length will decrease due to the loss of the first two rockers of stance [16]. Less severe contractions produce gait similar to that for dorsiflexor weakness, affecting only IC and swing [16].

Moderate soleus and gastrocnemius spasticity and co-contraction when the knee is extended, causes excessive plantar flexion throughout stance, but not during swing [16].

2.2.2 Excessive Dorsiflexion

Excessive dorsiflexion affects stance phase functions. IC still involves heel contact, however, the heel rocker is exaggerated, leading to sagittal plane instability [16]. The lack of plantar flexion at LR results in greater tibial rotation about the heel rocker, causing greater knee flexion [16]. During MSt, ankle dorsiflexion through the second rocker is largely unaffected. However, an increased rate of dorsiflexion results in instability during single leg support contributing to increased knee flexion [16]. As the limb transitions to swing, excessive dorsiflexion may cause prolonged heel contact during TSt and PSw and limited power production or push-off.

The primary causes of excessive dorsiflexion at the ankle are plantar flexor weakness and ankle fixation. Plantar flexor weakness results in an inability to control forward progression through the ankle rocker, leading to rapid dorsiflexion over a larger range during MSt. The anterior orientation of the tibia throughout stance results in knee flexion, increasing the demand on the quadriceps muscles to prevent buckling [16]. The heel remains in contact through TSt, and knee extension is not possible. Restricted ankle range of motion (ROM) causes deviation from normal gait similar to excessive dorsiflexion due to the obstruction of normal plantar flexion throughout stance [16]. The rigid fixation between the foot and the tibia increases the heel rocker action; movement through the rocker brings the foot to full contact with the ground, carrying the tibia forward and flexing the knee during LR [16].

2.3 Current AFO Designs

The minimum functional goal of AFO users is to return to ambulation. Depending on the functional loss and needs of the patient, ambulation goals might range from household (single walking

speed over level ground) to community (multiple walking speeds; navigation of environmental barriers such as stairs, ramps, and uneven ground) ambulation. To achieve these goals, the functional objectives of the AFO are to stabilize the ankle and subtalar joints and ensure adequate floor clearance during swing phase, while minimally compromising progression through stance phase [2].

Two categories of AFOs, static and dynamic, have been developed to reduce gait pathologies. Static orthoses restrict movement in all planes, providing rigid stability and control of the ankle and subtalar joints [2]. While these devices provide rigid support, the full restriction of movement inhibits normal progression through the three rockers during the stance phase of gait [1, 2, 16]. To improve forward progression, dynamic AFOs permit limited motion in the sagittal plane, restricting plantar flexion during stance phase [1, 2]. These simple functional objectives can be addressed through thermoplastic and carbon fiber AFO designs, improving patient ambulation while maintaining light and cosmetically acceptable devices [1, 5].

2.3.1 Static Orthoses

The simplest static orthotic design is the solid-ankle AFO (Figure 4a), designed to hold the foot and ankle in a constant neutral position. The design encompasses the posterior and inferior surfaces of the shank and foot, limiting all motion [1, 18]. The resistances to plantar flexion in swing and dorsiflexion during stance are controlled by forces applied to the ankle, shank, and foot by the AFO surface, proximal strap, and footplate/shoe [2]. These localized forces create three-point bending moments in the sagittal plane, resisting ankle movement throughout the stance and swing phases of gait. The solid-ankle design is traditionally made of thermoplastics to allow for easy modification. The footplate trimline, proximal border, and proximal closure strap of the AFO can be adjusted to modify the location of the focal forces, changing the stabilizing bending moments [2]. Frontal plane motion is reduced via the localized medial-lateral AFO forces, proximal and distal to the malleoli. For increased stability against foot inversion/eversion, the anteroposterior and footplate trimlines can be extended [2]. Indications for

prescription of this AFO are excessive plantar flexion due to hypertonicity of the plantar flexors, impaired motor control of the ankle and knee, and/or frontal plane instability [2]. An additional candidate population is traumatic injury patients with severely limited ankle range of motion. The solid-ankle AFO corrects excessive plantar flexion by preventing all plantar flexion and provides increased overall stability at the ankle by restricting movement. These constraints, however, can cause compensatory deviations in gait, as described previously (Section 2.2.2).

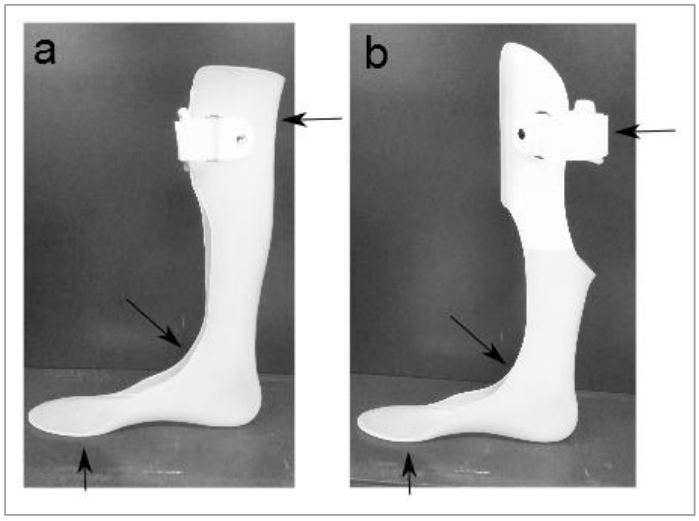

Figure 4: Three point bending forces promoting dorsiflexion in static AFO designs: a) solid-ankle AFO and b) ground reaction force AFO.

An alternative static AFO design is the ground reaction force (GRF), or anterior leaf spring, AFO (Figure 4b). Similarly to the solid-ankle AFO, the GRF AFO encompasses the posterior and inferior surfaces of the shank and foot, but includes a rigid anterior surface to resist tibia rollover (second rocker) during stance [2]. This additional constraint acts to improve knee stability, creating an external knee extensor moment during stance [2]. Ankle and subtalar joint stability mechanisms are the same as for the solid-ankle AFO [1, 2]; the stabilizing three-point bending moments are manipulated via modifications of the trimlines. The GRF AFO is prescribed to patients with plantar flexor and dorsiflexor weakness; its rigid structure prevents both excessive plantar flexion and dorsiflexion, as well as rapid tibial progression.

2.3.2 Dynamic Orthoses

To minimize gait deviations and assist forward progression, dynamic AFOs permit limited dorsiflexion during stance. One dynamic design, the posterior leaf spring AFO (Figure 5), is traditionally fabricated from thermoplastic materials, assisting rollover at the first rocker during loading response, as well as resisting plantar flexion during swing [2]; this device is used to counteract dorsiflexor weakness and impaired motor control [2]. Unlike the solid-ankle AFO, the posterior leaf spring design features shallow medial and lateral trimlines, reducing sagittal and frontal plane stability [2, 19, 20]. At IC and early LR, the flexibility of the posterior leaf spring aids foot deceleration, minimizing potential foot slap. During MSt, the device permits dorsiflexion, providing smooth tibia advancement through the second rocker of stance [2]. Though the AFO allows dorsiflexion, this motion requires deflection of the posterior "spring". During TSt and PSw the ankle begins to plantar flex, allowing the device to return to its original geometry, propelling the lower limb into swing. While the posterior leaf spring controls forward progression during stance, the foot is supported throughout swing, preventing plantar flexion and assisting foot clearance [1, 2]. The amount of rotational motion permitted at the ankle is dependent on the thermoplastic thickness and the trimlines of the posterior strut [2].

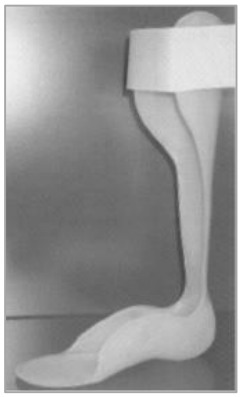

Figure 5: Posterior leaf spring AFO. Adapted from [2].

To further improve progression through stance, especially the second and third rockers, posterior leaf spring AFO designs have been adapted to incorporate carbon fiber materials, such as the Carbon

Ankle 7 AFO by Otto Bock (Duderstadt, Germany) (Figure 6a) [2]. In this design, a carbon fiber strut replaces the posterior thermoplastic leaf spring, providing enhanced energy storage from LR through MSt and energy release from TSt for PSw [2, 7, 8, 21]. The carbon fiber spring is typically L-shaped, with the base attached to the plantar surface of the thermoplastic footplate and the upright attached to the posterior surface of the proximal thermoplastic cuff [2]. The enhanced energy response is due to the material properties of the carbon fiber; increased stiffness requires more force to deform the carbon fiber strut and returns greater force as it returns to its original shape. The stiffness of the carbon fiber spring is generally selected based on the patient's weight and activity level, though springs of varying stiffness may be substituted to accommodate different activities [2]. Alternatively, posterior leaf spring AFOs can be fabricated from a single carbon fiber sheet, such as the PhatBrace "Dynamic Response AFO" by Bio-Mechanical Composites (Des Moines, IA) (Figure 6c) [22]. These devices provide biomechanical assistance similar to a posterior leaf spring AFO and are also prescribed for individuals with dorsiflexor weakness. Candidates for carbon fiber AFOs typically have better motor control and improved functional outcomes, such as community ambulation.

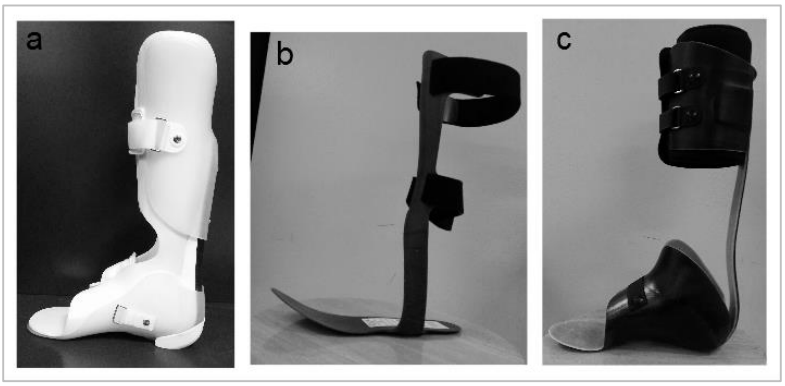

Figure 6: Carbon fiber AFO designs: a) Carbon Ankle 7 strut in a thermoplastic design, b) BlueRocker™ commercial design, and c) PhatBrace Dynamic Response AFO.

Dorsiflexion-assist AFO designs, such as the BlueRocker™ AFO (Allard USA, Inc.; Rockaway, NJ) may also be fabricated from a single carbon fiber sheet, linking the cushioned anterior shin piece to a full footplate with a medial upright (Figure 6b). The shin piece is secured to the shank using straps,

allowing for a slim, aesthetic design. These orthoses control plantar flexion at IC and LR, allowing tibial progression during MSt, and assisting push-off during TSt through PSw [2, 9].

2.3.3 Intrepid Dynamic Exoskeletal Orthosis (IDEO)

While thermoplastic and carbon fiber designs improve gait and provide ankle and subtalar joint stability, energy storage and return of these devices is insufficient for high-intensity activities such as running and jumping [7, 8, 11]. The Intrepid Dynamic Exoskeletal Orthosis (IDEO) facilitates return to high-intensity activity for patients with limited neuromuscular control and reduced ankle range of motion [10]. Developed by the Center for the Intrepid (San Antonio, TX), the IDEO was designed for military professionals who have undergone limb salvage surgery after high-energy traumatic injuries [10]. While limb salvage surgery provides an alternative treatment option to amputation, most surgeries result in ankle fusion, severely restricting "pain-free" ankle motion. Prior to the development of the IDEO, these physically fit military patients, accustomed to participation in high-intensity activities, were prescribed static AFOs. However, as noted previously, the static AFO designs interfere with the three rockers of stance, adversely affecting gait and prohibiting running and other activities.

The IDEO (Figure 7) is a novel orthosis that maintains a fixed ankle position while providing adequate energy storage and return for high-intensity activities. The design integrates carbon graphite pylon struts with a carbon fiber proximal ground-reaction cuff and distal supramalleolar ankle-footplate. Inspired by prosthetic running feet such as the Cheetah (Otto Bock; Duderstadt, Germany), the footplate is typically aligned in a plantar flexed orientation, within the "pain-free" ankle ROM, and includes a rocker sole, aiding motion over the forefoot rocker and energy transfer [11]. The plantar flexed foot position and posteriorly offset carbon fiber struts, similar to the alignment of prosthetic running feet, are presumed to increase strut deflection from midstance to terminal stance; the design parameters serve to minimizing ankle motion (and pain), while storing and returning energy throughout stance. The stiffness of the carbon fiber struts can also be adjusted to meet each patient's needs [23]. While use of the IDEO

has resulted in improved functional performance clinically [10-12, 24], the mechanical behavior of this device is poorly understood.

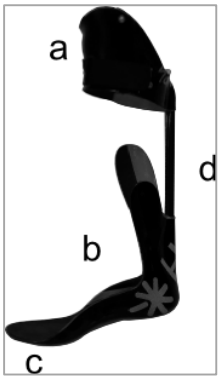

Figure 7: The current IDEO design, composed of: a) carbon fiber proximal cuff, b) footplate, c) rocker sole, and d) carbon graphite pylon system struts.

2.4 Mechanical Testing of AFOs

The fabrication material, thickness, and trimlines of AFO designs are modified by certified orthotists to adjust the biomechanical behavior of the AFO-limb complex for each patient. The mechanical properties of the AFO include specific material properties (e.g., Young's modulus, shear modulus, Poisson's ratio, ultimate stress, yield stress) as well as structural properties (e.g., fracture strength, stiffness) influenced by design geometry. One mechanical characteristic previously investigated is orthotic stiffness or structural stiffness, which includes both rotational stiffness and compressive stiffness characterization, as discussed previously (Chapter 1). Orthotic stiffness is used to quantify the assistance of, or resistance to, dorsi-/plantar flexion from IC through push-off via force-displacement (compressive) and/or moment-angle (rotational) curves [14]. Orthotic stiffness measures are dependent on the specific mechanical testing techniques used.

2.4.1 Technique

Functional testing assesses the behavior of the AFO and lower limb of an individual patient together; calculated stiffness of the AFO-limb complex includes passive, viscoelastic resistance of the limb in addition to the device's inherent orthotic stiffness [25, 26]. Rotational stiffness is determined by characterizing the moment-angle curves for the lower limb with and without an AFO [25]. Experimental methods typically hold the shank fixed as an instrumented lever attached to the foot-footplate complex rotates about an axis coincident with the ankle joint axis (Figure 8). Kobayashi et al. used a torque meter and potentiometer to directly measure the moment and angles of the AFO-limb complex at the ankle [26]. Similarly, physical therapy exercise systems (e.g., kinematic dynamometer such as Cybex) have also been used to control motion and acquire moment-angle data [25]. While the stiffness of the AFO-limb complex is an important parameter affecting gait, this integrated mechanical behavior is dependent on the unique physiology of each subject, making functional testing results of the AFO-limb complex highly variable and difficult to extrapolate to other populations.

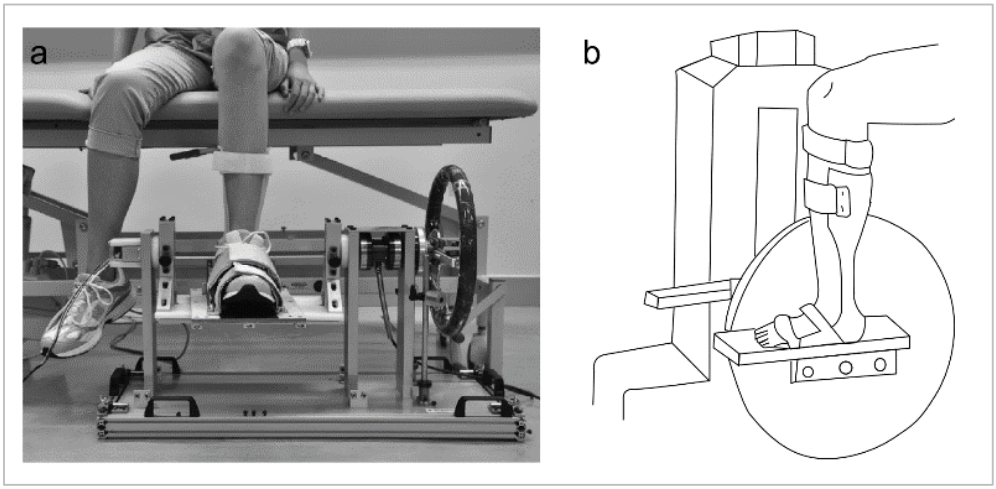

Figure 8: Functional AFO mechanical testing apparatus where a) rotating footplate is manually deflected [26], and b) footplate is rotate using a kinematic dynamometer [25].

Bench testing is the more common approach to AFO testing as it does not require human subjects and uses a controlled testing environment that is independent of individual physiology. For mechanical testing of most traditional AFO designs, stance phase during gait is simulated by loading either the proximal cuff or footplate, causing rotation between the foot/footplate and shank/posterior support segments. Previous investigations which used bench top mechanical testing to characterize orthotic stiffness, rotational and/or compressive, included various methodologies and techniques (Figure 9) (Table 1).

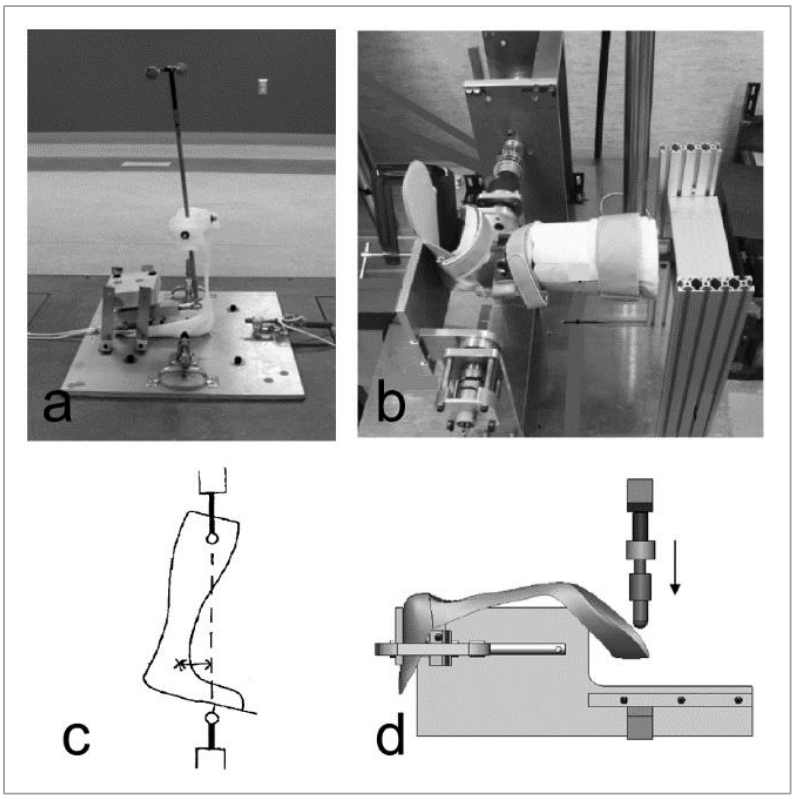

Figure 9: Static (a & b) and dynamic (c & d) AFO mechanical bench testing techniques. Adapted from [27-30].

Table 1: Summary of mechanical testing of AFO-limb complexes. PF: plantar flexion, DF: dorsiflexion

Reference	Technique	Load Sharing Device	Deflection Application	Range of Motion	Test Method	Metric	Sensors	AFOs Tested
Yamamoto – 1993 [25]	Functional Testing	Patient limb	Automated rotation	20° PF – 15° DF	Dynamic	Rotational stiffness	Muscle training machine	Posterior/Anterior leaf spring, Spiral (thermoplastic)
Kobayashi – 2011 [26]	Functional Testing	Patient limb	Manual	N/A	Dynamic	Rotational stiffness	Torque meter Potentiometer	N/A
Singerman – 1999 [31]	Bench Testing	Partial shank surrogate limb	Manual	10° PF – 10° DF	Dynamic	Rotational stiffness	Strain gages Motion analysis	Solid-ankle, Posterior leaf spring, Hinged (thermoplastic)
Cappa – 2003 [14]	Bench Testing	Endoskeletal surrogate limb	Manual	6° PF – 6° DF	Dynamic	Rotational stiffness	Load cells Rotary optical encoders	Spiral
Novacheck – 2007 [27]	Bench Testing	Partial shank surrogate limb	Manual	20° PF – 20° DF	Dynamic	Rotational stiffness	Force plate Motion analysis	Posterior leaf spring (thermoplastic and carbon fiber)
Bregman – 2009 [32]	Bench Testing	Endoskeletal surrogate limb	Manual	10° PF – 20° DF	Dynamic	Rotational stiffness	Load cells Joint angle sensors	Solid-ankle, Posterior leaf spring (thermoplastic and carbon fiber)
Ringleb – 2009 [33]	Bench Testing	Full surrogate limb	Automated rotation	1-9° DF 3-10° PF	Dynamic	Rotational stiffness	Load cell Tilt sensor	Arizona AFO
Kobayashi – 2010 [28]	Bench Testing	Partial shank surrogate limb	Automated rotation	15° PF – 15° DF	Dynamic	Rotational stiffness	Torque meter Potentiometer	Articulated thermoplastic
Major – 2004 [29]	Bench Testing	None	Automated compression	0° DF – 10° DF	Pseudo-static	Rotational stiffness	Mechanical testing machine	Solid-ankle (thermoplastic and carbon fiber)
Hawkins – 2010 [30]	Bench testing	None	Automated compression	0.5, 1, 1.5, 2 inch maximum displacement	Pseudo-static	Compressive stiffness	Mechanical testing machine Strain gages Deflectometer	HELIOS AFO

2.4.2 Load Sharing Devices

To simulate ambulatory loading of the AFO-limb complex, many bench testing methods incorporated a partial or full surrogate limb [14, 27, 28, 31-33]. A partial surrogate limb typically consists of a surrogate shank with an internal rod, or tibia-fibula complex, exclusive of a foot and ankle construct (Figure 10b). The AFO is positioned around the surrogate shank; loads are applied to the orthotic footplate. A full surrogate limb includes a surrogate shank, foot, and articulating ankle (Figure 10a and c). The advantage of a full surrogate limb is the explicit ankle articulation between the shank and foot segments, which can be instrumented to measure ankle position [32]. An ideal surrogate limb integrates a properly aligned ankle joint with a shank that incorporates a rigid internal structure surrounded by a compliant viscous/viscoelastic material simulating the surrounding bulk soft tissue [13]. Bench testing with a more biofidelic surrogate limb can improve the repeatability of measurements and provide better understanding of the relationship between an AFO and lower limb that can be more readily extrapolated to actual AFO/patient populations.

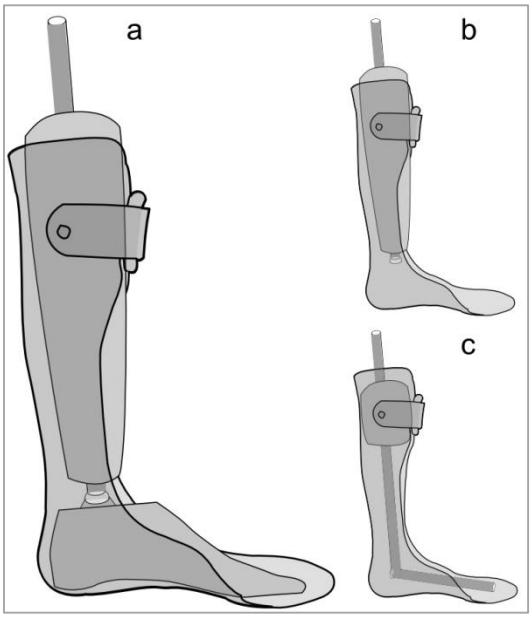

Figure 10: Load bearing devices: a) full surrogate limb, b) partial shank surrogate limb, and c) endoskeletal surrogate limb.

2.4.3 Deflection Application

To characterize AFO stiffness, mechanical testing protocols involve inducing a vertical or rotational deflection to the AFO while measuring the resultant force or torque, respectively. In several studies, either the proximal or distal segment of the AFO was rigidly fixed; the free segment was manually rotated in the sagittal plane [14, 27, 31, 32]. Manual application of deflection is difficult to constrain to the sagittal plane, and often induces rotation at the talorcrural joint in the frontal plane [14]. While loading velocity does not appear to have a significant impact on measured stiffness [25], constant loading rates are difficult to apply manually.

Alternatively, automated methods have been implemented using material testing machines to apply rate-controlled vertical or rotational deflections [28-30, 33]. The orientation of the AFO in a compressive materials testing machine is varied to apply the desired bending moment about the center of rotation. Both cantilever beam setups [30] and angular offset orientations [29] have been implemented. Kobayashi et al. modified a mechanical testing machine to incorporate a rack and pinion system to convert vertical displacement of the loading nose to rotational motion of the attached footplate [28]. A two-axis gimbal has also been used to automate rotational deflection [33].

2.4.4 Test Method

Dynamic bench testing protocols typically characterize the moment-angle relationship across a continuous range of ankle angles in the sagittal plane. To simulate the forces and moments observed during gait, displacement is typically applied to the footplate or proximal support through a range of clinically relevant ankle/AFO orientations [14, 27, 28, 31-33].

In addition to dynamic testing methods, pseudo-static bench testing methods have also been used to assess rotational and compressive stiffness, applying a compressive bending moment about the AFO ankle. During pseudo-static bench testing, the AFO is oriented to approximate an instance in the gait cycle; compressive load at a constant loading rate is applied using a mechanical testing machine until a prescribed force is imposed (Figure 9c) [29, 30]. The corresponding final vertical displacement is then used to calculate the angular displacement at the ankle [29]. Without directly measuring ankle angle, however, these indirect angular position estimates are subject to error as the shank and foot sections of the AFO are not rigid segments. An alternative pseudo-static testing protocol used a cantilever beam arrangement to position the AFO horizontally with respect to the mechanical testing machine (Figure 9d) [30]; this protocol incorporated similar methods to estimate angular position. While these mechanical testing procedures facilitate measurements of AFO stiffness, the ankle range of motion investigated often does not span the full functional range (15° plantar flexion to 15° dorsiflexion) [28]. As dynamic testing demonstrated that AFO stiffness is dependent on ankle angle [28, 31], characterization of AFO stiffness should incorporate the full ankle range of motion throughout stance phase.

2.4.5 Sensors

The specific mechanical metric of interest (e.g., compressive or rotational stiffness) determines the desired measurands (Table 1). For example, quantification of compressive stiffness requires a measurement of both force and displacement. These measurands might be evaluated using the load cell and optical encoder of a mechanical testing machine [30]. Rotational stiffness requires measurement of moment and angle. Moment can be directly assessed using a torque meter, or indirectly using strain gaged load cells or force plates and the corresponding lever arm [14, 27-29, 31-33]. Angular measures of the ankle joint or AFO have most commonly been measured using motion analysis [27, 31], although other rotation sensors (optical rotary encoders [14], tilt sensors [33], and potentiometers [28, 32]) provide similar measurements.

2.5 Summary

This chapter presented an overview of able-bodied and pathologic gait, focusing on ankle and foot kinematics and kinetics. Current AFO designs were summarized, detailing design parameters and adaptations, biomechanical functional impact on gait, and prescription criteria. A new AFO, the IDEO, was introduced as an alternative orthotic solution for patients with limited ankle motion with high activity functional goals. Finally, methodologies for mechanical testing of AFOs were reviewed, contrasting the benefits and limitations of various protocols.

CHAPTER 3: METHODOLOGY

AFOs of different materials and designs were tested to compare their mechanical behaviors and to develop a mechanistic model to better understand the functional outcomes observed clinically. To characterize the structural stiffness and rotational motion of each AFO, the orthoses were donned on a surrogate limb and compressively loaded to simulate instances during stance phase of gait. An inductive ankle angle sensor was designed and included to measure ankle rotation of the surrogate limb. In conjunction with the mechanical testing, motion analysis was used to quantify the deflection of the posterior strut and relative rotation of the proximal and distal sections of each AFO. The mechanical testing and data collection were completed in two phases, the first characterizing compressive stiffness and posterior strut deflection, and the second investigating rotational motion of the AFO and surrogate ankle.

3.1 Tested AFOs

Seven different AFOs, described in Section 2.3, were investigated in this study: an IDEO, four carbon fiber AFO designs (PhatBrace Dynamic Response AFO; thermoplastic AFO with Otto Bock Carbon Ankle 7 struts of two different stiffness; BlueRocker™), and two traditional thermoplastic AFO designs (GRF AFO and solid-ankle AFO). These AFOs were selected for comparison to the IDEO due to their incorporation of similar materials (e.g., carbon fiber PhatBrace and BlueRocker™), similar prescription criteria (e.g., solid-ankle AFO, GRF AFO and Carbon Ankle 7 AFO), and/or similar restricted range of ankle motion (e.g., solid-ankle AFO and GRF AFO).

One female human subject, a candidate for the IDEO, was identified from the Milwaukee Hanger Prosthetics & Orthotics client database and served as the model for the respective AFOs and surrogate limb. Details regarding this subject are summarized below.

Body weight	800 N (180 lbs)
Height	172.7 cm (68 in)
Cause of injury	Motor-vehicle collision
Injury	Right tibial fracture
Functional deficits	Plantar flexion and dorsiflexion weakness

The right limb of this subject was casted by a certified orthotist (T. Current, Hanger Prosthetics & Orthotics, Milwaukee, WI). This cast was used for fabrication of the custom AFO designs (solid-ankle, GRF, IDEO, Carbon Ankle 7, and PhatBrace) and for the surrogate limb model. The off-the-shelf AFO (BlueRocker^{TM}), sized for this subject, and the PhatBrace Dynamic Response AFO, fabricated by Bio-Mechanical Composites, Des Moines, IA, were ordered based on subject anthropometry. An orthotist (T. Current, Hanger Prosthetics & Orthotics, Milwaukee, WI) fabricated the solid-ankle AFO, GRF AFO, and Carbon Ankle 7 AFO as per clinical guidelines (Hanger National Labs, Orlando, FL); a second orthotist (R. Blanck, Hanger Prosthetics & Orthotics, Tacoma, WA) fabricated the IDEO from a second cast of the subject, specific for the IDEO.

3.2 Surrogate Limb Model

A surrogate limb was constructed to form an internal support structure, approximating the test subject's lower limb, for the AFOs during mechanical testing. The load sharing device used is similar to those in literature [27, 28, 31], with the inclusion of a foot/ankle to observe ankle rotation during loading. This surrogate limb consisted of a single-axis prosthetic foot/ankle (Ohio Willow Wood Co.; Sterling, OH), a pseudo-skeletal aluminum "shank" pylon (TruLife; Hannover, Germany), a surrounding rigid foam cover (SPS National Labs; Tempe, AZ), and an

external gel liner (Alps South LLC; St. Petersburg, FL) (Figure 11). The foam cover, used to approximate the soft tissue bulk, was formed from the same cast used to fabricate the AFOs with a global 3 mm circumferential reduction to account for the thickness of the gel liner. The distal and proximal portions were removed such that the surrogate shank spanned the mid-patella to mid-malleoli region. A central core was drilled to accommodate the pylon; the single-axis foot/ankle was connected to the shank pylon using a tube clamp/pyramid adapter. To minimize slip of the foam relative to the pylon, an expanding foam (Dow Chemical Company; Midland, MI) was inserted around the distal and proximal pylon borders. The superficial gel liner was pulled over the rigid foam to simulate the compliant, viscoelastic skin and soft tissue at the skin-AFO interface.

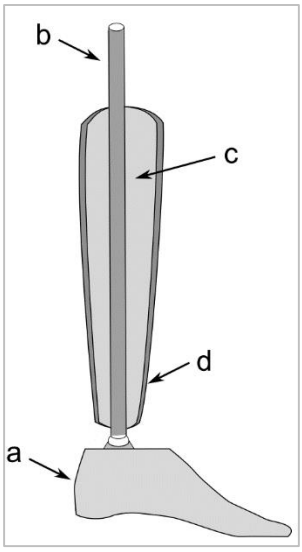

Figure 11: Surrogate limb design: a) single-axis prosthetic foot-ankle, b) aluminum pylon, c) foam shank, and d) gel liner

3.3 Mechanical Testing Configuration

Each AFO was donned over the surrogate limb model for mechanical testing. Pseudo-static bench testing of each AFO-surrogate limb complex was conducted using materials testing systems (MTS 809 Axial / Torsional load frame, single axis 44.5 kN load cell, running FlexTest

4.0 for strut displacement testing, or MTS Criterion, single axis 5kN load cell, running TestWorks 4.0 for AFO rotation testing, MTS Systems Co.; Eden Prairie, MN). Bench testing eliminated variability inherent to functional testing of human subjects. The materials testing system ensured controlled, repeatable application of vertical displacement, as well as accurate measurement of the resultant load. The materials testing system, however, required pseudo-static displacement application, rather than dynamic loading, to approximate gait.

To approximate AFO-limb loading during gait, pseudo-static loading corresponding to various instances in the gait cycle was applied. Both the load magnitude and direction vary during stance, as does the limb orientation. The specific AFO-surrogate limb complex loading protocol was based on level walking data for an age- and weight-matched able-bodied subject (Center for Motion Analysis; Greenfield, WI). Kinematic data were collected using Vicon Nexus (Version 1.8.5, Vicon Motion Systems, Lake Forest, CA) during level overground walking trials. Data from a singular trial with clear foot strikes on each force plate were used. The angle between subject's shank and vertical reference (global coordinate system) was calculated using malleolar and femoral condyle marker locations. Ground reaction force data were synchronously acquired via force plates (AMTI OR6-5, Watertown, MA and Bertec FP4060, Columbus, OH). Heel strike and toe off events were detected in Vicon and various sub-phases of stance were identified using kinematic and kinetic data (Figure 12). Within each sub-phase, a discrete shank to vertical angle and corresponding vertical force magnitude was selected as a testing condition (Table 2).

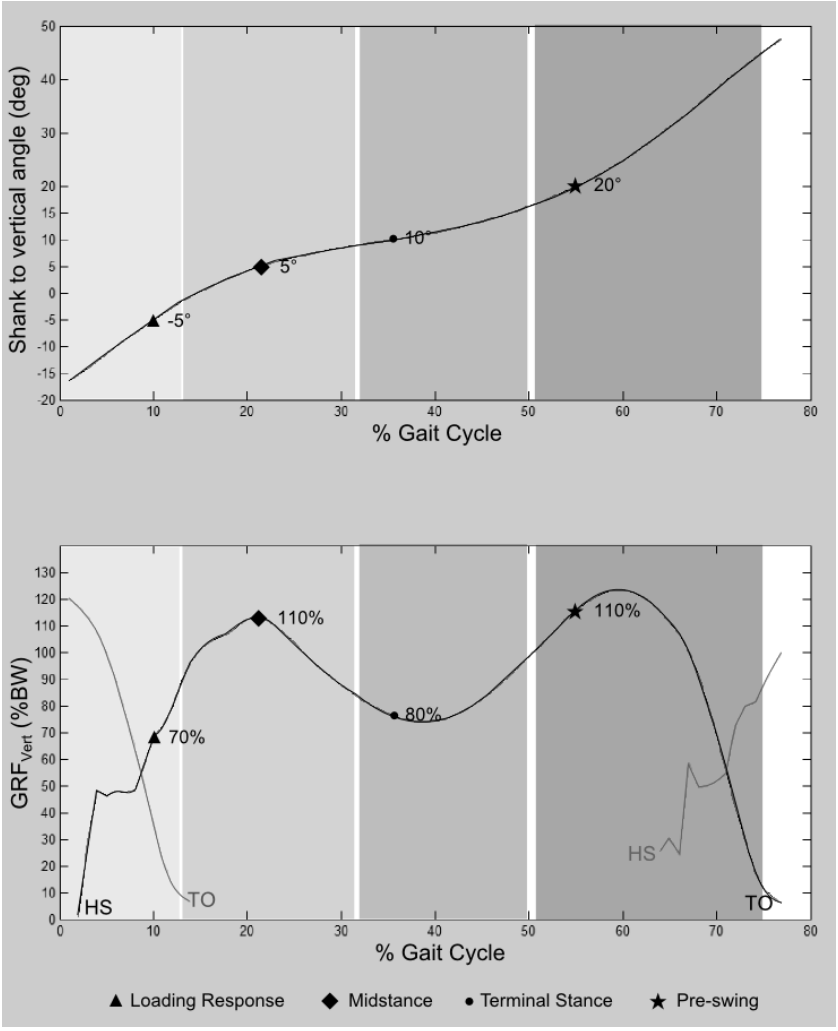

Figure 12: Shank-to-vertical angle and vertical ground reaction force, as percentage of body weight, of a normal, age-matched able-bodied subject during stance (Center for Motion Analysis; Greenfield, WI). The various sub-phases of stance are shaded and both heel strike (HS) and toe off (TO) events are labeled.

Table 2: Discrete testing orientations and loads corresponding to different sub-phases of stance.

Stance Sub-Phase	Shank to Vertical Angle (°)	Vertical Force (% Body Weight)	Actual Force (N)
LR	-5	70	560.5
MSt	5	110	880.7
TSt	10	80	640.5
PSw	20	110	880.7

To apply loads at the appropriate limb orientation, the AFO-surrogate limb complex was positioned within the materials testing machine using an adjustable loading plate (Figure 13). The proximal end of the pylon of the surrogate limb was inserted into the upper grips of the MTS, facilitating load application directly to the "skeletal" structure of the surrogate limb. This test protocol was based on the test methods for evaluating prosthetic foot design [34].

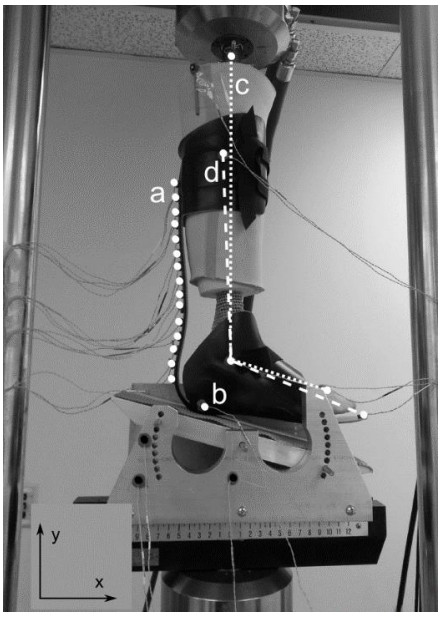

Figure 13: Mechanical testing setup with proximal fixation, adjustable loading plate, and markers at: a) posterior strut, b) loading contact point, c) AFO ankle angle, and d) limb ankle angle.

For the mechanical bench testing, a specific AFO was donned over the surrogate limb. To maintain proper contact between the BlueRocker^{TM} AFO and the surrogate limb, a sandal (Nike ACG ORS-044, size US 8) was strapped over the prosthetic foot and AFO footplate. The AFO-surrogate limb complex was then secured in the materials testing machine, aligned as for LR. A pre-load of 66.7 N (15 lbf) [34] was applied to ensure proper seating of the surrogate limb within the orthosis, accommodating potential laxity in the system and minimizing settling during testing. Cyclic loading (10 cycles to the target load in Table 2) were applied at a randomly selected displacement loading rate of 5 mm/s or 10 mm/s. The displacement loading rates were

chosen within the range of previous mechanical testing protocols [29, 30] to approximate normal and fast-paced walking, respectively, and investigate potential rate dependence. All signals (force and displacement, marker motion, and inductance sensor) were acquired at 115 Hz, the maximum sampling frequency of the Optotrak system, on separate computers. Data were synchronized post-acquisition (see Section 3.6.1). This testing protocol was repeated for each of the sub-phases of stance investigated (i.e., MSt, TSt, and PSw).

Kinematic data were acquired to quantify the deflection of the AFO posterior strut, as well as effective rotation of proximal and distal orthosis segments. The active marker motion tracking system (Optotrak Certus running NDI First Principles, NDI; Ontario, Canada) was used for all motion analysis.

3.4 Compressive Stiffness and Posterior Strut Deflection Testing

The first phase of testing (Figure 14) was conducted to characterize the compressive stiffness, posterior strut deflection mechanism, and rotational stiffness. During an initial trial, the target load (Table 2) was applied to the AFO-surrogate limb complex. The vertical displacement corresponding to the target load position was used as the target displacement for the MTS FlexTest 4.0 *displacement controlled* protocol. To minimize potential damage to the orthosis and footplate contact anomalies, the test load, and thus target displacement, was reduced if either of the following conditions was met: 1) the vertical limb-orthosis displacement exceeded 2.54 cm, or 2) midfoot contact shifted by more than 20% of the midfoot length (2.8 cm). The vertical displacement limitation was chosen to prevent damage to the AFOs. The latter criterion ensured that the experimental test conditions authentically approximated normal loading and contact during gait. In addition, as the ankle lever arm (ankle center to rotation to foot contact

region) was used to estimate ankle moment, inconsistent mid-or fore-foot contact would induce errors in ankle moment calculations.

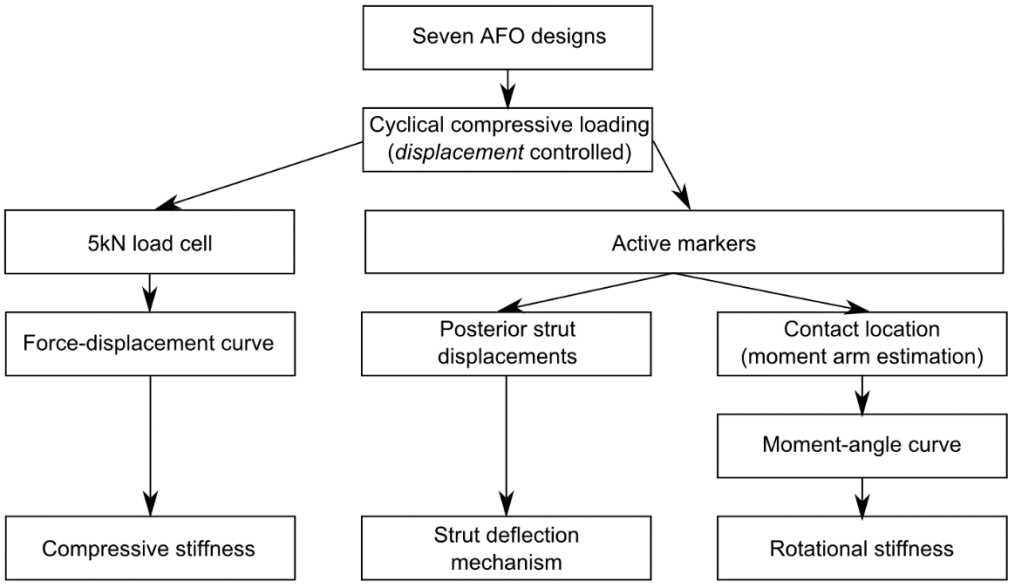

Figure 14: Compressive stiffness and strut deflection testing design including AFO designs tested, sensors used, and parameters analyzed.

To quantify AFO strut deflection during pseudo-static loading, 15 active markers (7 mm diameter) were placed along the AFO posterior strut at 2 cm increments (Figure 13). For the GRF AFO, strut markers were placed on both the distal posterior strut as well as on the proximal anterior surface of the cuff, at 2 cm increments. Additional markers were placed on the proximal lateral flare (along the central longitudinal axis) and the anterior footplate of the AFO. Markers were also positioned on the surrogate limb: over the exposed proximal pylon, the proximal foam shank, the malleoli of the prosthetic foot shell, and the metatarsal head region. The malleoli of the prosthetic foot shell approximated the surrogate limb ankle axis of rotation. For the solid-ankle, GRF, Carbon Ankle 7, and PhatBrace AFOs, the malleoli were obscured; the ankle axis of rotation was approximated by a marker positioned over the proximal lateral flare of the orthosis.

A single marker was placed at the approximate contact point between the AFO and the loading plate. A global, laboratory-based coordinate system was defined by markers placed on the adjustable footplate fixture.

3.5 AFO and Underlying Ankle Rotation Testing

3.5.1 Testing Setup

The second phase of testing (Figure 15) was conducted to characterize the compressive stiffness, AFO segment rotations, and motion of the underlying ankle complex.

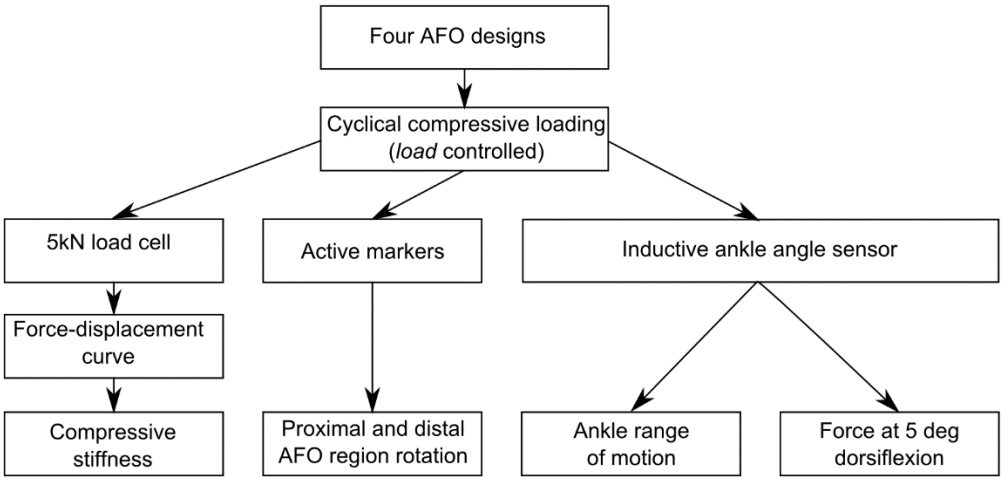

Figure 15: AFO and ankle rotation testing phase design including AFOs tested, sensors used, and outcome measures.

Four of the seven AFOs (solid-ankle AFO, GRF AFO, IDEO, and PhatBrace Dynamic Response AFO) were also tested to assess rotational motion and stiffness. The Carbon Ankle 7 and BlueRocker™ AFOs were excluded from the additional testing as the prescription criteria and compressive stiffness of these orthoses differ from the IDEO.

The target loads (Table 2) were used as an indicator for the MTS TestWorks 4.0 *load controlled* protocol. AFOs were tested to the full test load for each stance sub-phase, regardless of changes in plantar surface contact area, to characterize the full range of rotational motion.

To quantify the effective AFO rotation, the proximal cuff and distal foot plate were considered independent rigid segments. Rigid orthogonal triads were constructed via 3D printing to support active markers of the respective segments. Five triads were fixed to the AFO (proximal cuff, hind foot and forefoot) and surrogate limb (shank pylon and second metatarsal region of the prosthetic foot) (Figure 16). The triads were secured to the AFO by drilling through the AFO structure, taking care not to affect AFO structural integrity. The surrogate limb triads were drilled through the proximal pylon and the foam shell of the prosthetic foot.

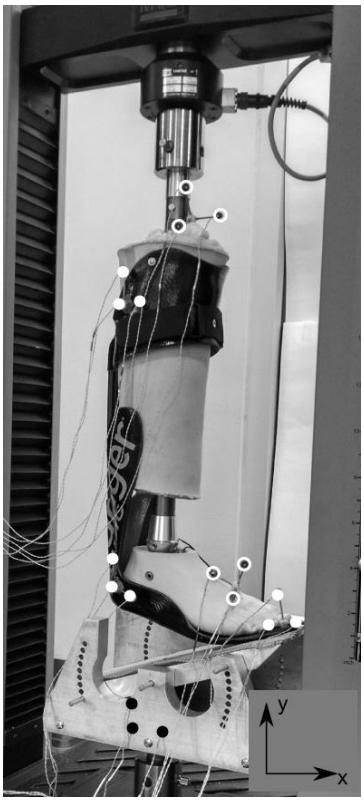

Figure 16: Mechanical testing setup and marker triad locations for rotational motion assessment. Filled markers represent the proximal, supramalleolar, and toe regions of the AFO; hollow markers approximate the proximal and foot segments of the surrogate limb.

3.5.2 Ankle Rotation Sensor

To explicitly quantify ankle rotation of the single-axis prosthetic ankle-foot of the surrogate limb model, an inductive rotation angle sensor was designed, fabricated, calibrated, and incorporated.

The ankle sensor was designed to measure the rotation of the single-axis prosthetic ankle. An inductor coil (insulated AWG 30 copper wire, 18 mm diameter, 18 turns) was attached to the underside of the ankle complex such that the plane of the coil passes over a ferrous rod (9.57 mm diameter, 2.4 mm length) of powdered iron secured to the internal foot base (Figure 17). The inductance coil translates along the rod as the ankle flexes/extends (Figure 18). The rod acts as the iron core of the inductor; as the coil translates along the rod the inductance of the coil changes. A function generator (Agilent 33120A, Agilent Technologies Inc.; Loveland, CO) supplied a sinusoidal input signal (10 V_{pp}, 1.9 MHz, resonant frequency of coil) to the inductance coil; ankle rotation resulted in proportional changes in current and observed voltage amplitude. A half wave rectifier-envelope detector circuit was incorporated to produce a proportional DC voltage output that varied nonlinearly with ankle angle (Figure 19). This output voltage was sampled at 115 Hz, consistent with the active marker data, using NI DAQ USB-6008 and LabVIEW software (National Instruments; Austin, TX). Analog voltage output from the load cell output was simultaneously acquired at 115 Hz using the same DAQ card. A schematic of the ankle sensor circuitry is included in Appendix B.

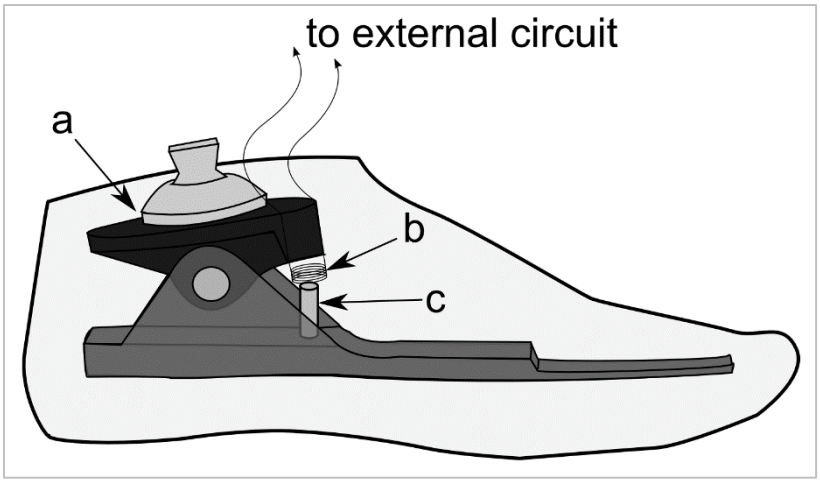

Figure 17: An inductive ankle sensor was incorporated in the prosthetic ankle-foot of the surrogate limb. Prosthetic ankle complex (a) rotation results in translation of the inductive coil (b) along the ferrous rod (c) to alter the input voltage signal.

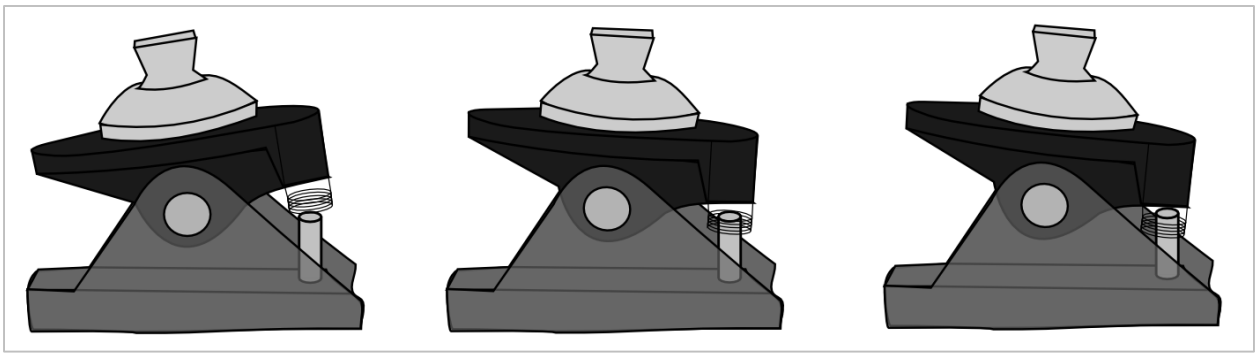

Figure 18: Close-up of rotational motion of the ankle complex and the corresponding translation of the inductive coil along the ferrous rod. The progression of motion shown results in increasing inductance of the coil.

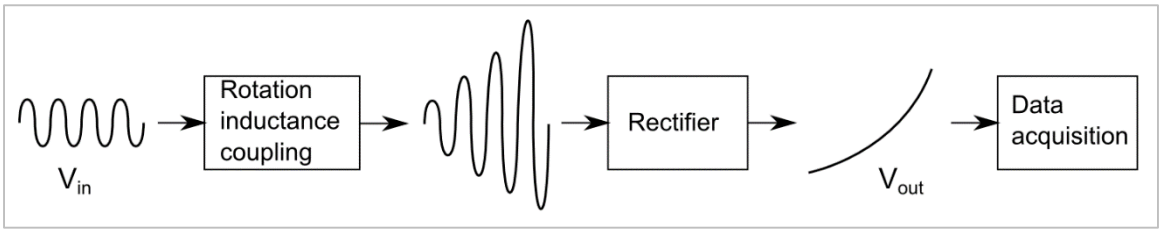

Figure 19: Schematic of the respective signal conditioning of the ankle inductance sensor prior to data acquisition.

The angle sensor was calibrated to quantify sensor linearity and generate a calibration curve such that future voltage output might be converted to ankle angular position. Active marker triads defining the rigid shank and foot segments, were respectively positioned on the shank pylon, and prosthetic forefoot; a single marker was placed on the prosthetic ankle axis of rotation. Sagittal plane vectors, defined from the ankle axis of rotation to the midpoint of the triad markers, were used to calculate the corresponding surrogate limb ankle angle (Figure 20). During the calibration trials, the surrogate foot was fixed to the ground as the pylon shank was manually rotated, imposing ankle rotation ranging from 15° plantar flexion to 15° dorsiflexion (e.g., range of motion of the ankle during gait [28]), relative to a neutral ankle angle of 90°.

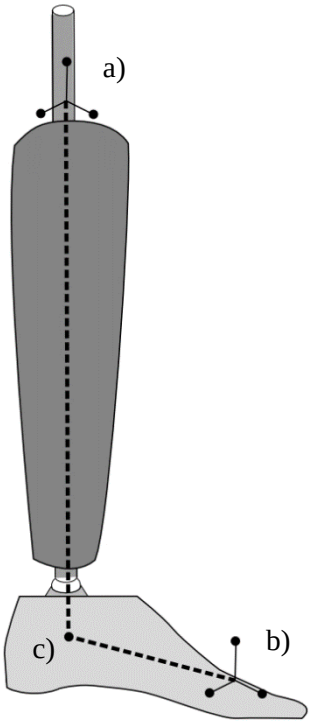

Figure 20: Marker setup for ankle sensor calibration data collection: a) shank triad, b) foot triad, and c) ankle center of rotation. The segment used to define the ankle angle are denoted by dashed lines.

The resultant voltage versus angle data from four rotational cycles were segmented into dorsiflexion and plantar flexion motions. As mechanical testing imposed dorsiflexion on the AFO-surrogate limb complex, only the dorsiflexion motion data were fit to a fifth order polynomial:

$$\Theta = 0.04x^5 - 0.67x^4 + 4.40x^3 - 13.62x^2 + 22.76x - 19.10 \quad (1)$$

where x is the voltage output (V) from the angle sensor and Θ is the ankle angle measured from motion analysis (°). The maximum error between the ankle angles determined by the active markers and the ankle angles determined with inductive angle sensor and Equation 1, 1.76°, occurred at approximately 11° plantar flexion (Figure 21).

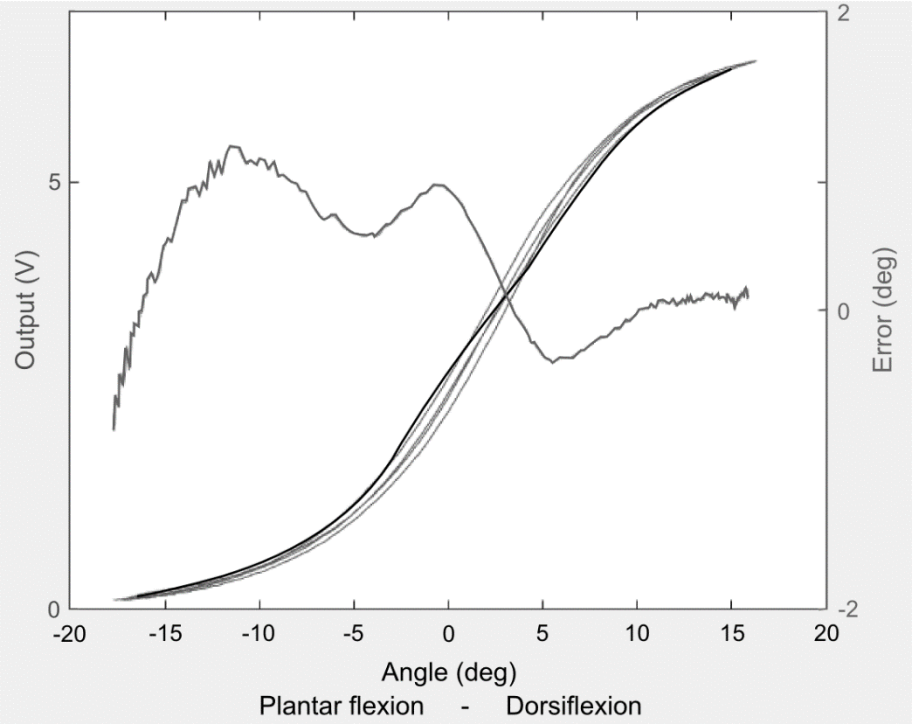

Figure 21: The angle sensor calibration data (grey) during manually imposed rotation of the surrogate limb, fit with a 5th order polynomial (black). The mean sensor error (right axis) as a function of ankle angle is also shown.

The dorsiflexion motions were also fit with a spline curve using a curve fitting tool (MATLAB R2013b, Mathworks; Natick, MA). The maximum error between the spline

calibration curve and the dorsiflexion calibration data was 1.47º, occurring at 3º of plantar flexion (Appendix B, Figure 38).

3.6 Data Analysis

All data processing was performed using MATLAB (MATLAB R2013b, Mathworks; Natick, MA).

3.6.1 Data Processing

For all trials, the force-displacement and marker motion data were synchronized post-acquisition, aligning the changing displacement in the force-displacement data files with the changing vertical displacement of the active markers on the footplate. The displacement maxima and minima of the loading crosshead were used to segment these data into loading/unloading regions.

For the AFO rotation trials, the force and ankle sensor data were collected synchronously on a third computer. The MTS force (analog output from MTS) was synchronously acquired using the USB DAQ. These force voltage data were used to segment the data into loading/unloading regions.

For both the force-displacement and force-angle data, the initial five cycles were discarded to eliminate potential pre-conditioning effects.

3.6.2 Compressive Stiffness Analysis

Force and vertical displacement of the AFO-surrogate limb complex during loading were averaged over the latter five cycles and utilized to assess compressive stiffness for each stance sub-phase for each AFO. Linear regression was performed on the initial and final 25% of the

mean force-displacement curves. The resultant slopes characterized the initial and final compressive stiffness of the AFO for a given stance sub-phase (Figure 22). The hysteresis or area between the mean loading/unloading data was calculated as the difference between the areas under the loading and unloading curves using trapezoidal approximation (Figure 23). The presence of hysteresis suggests that energy is lost during testing.

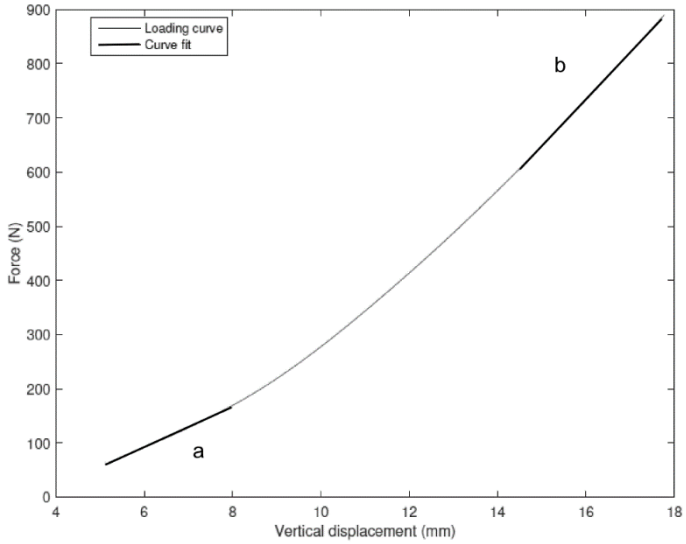

Figure 22: Mean force-displacement data during loading (grey) with initial (a) and final (b) linear regressions (black) to characterize compressive stiffness.

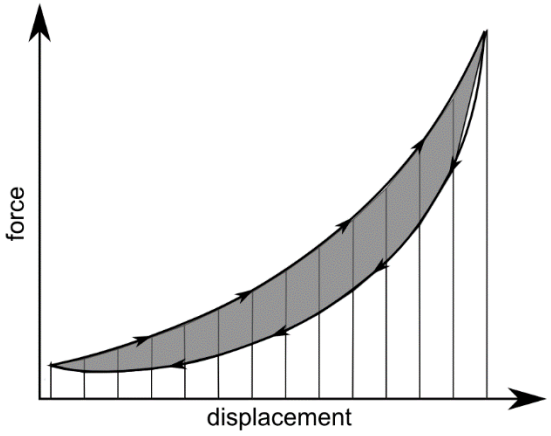

Figure 23: Hysteresis, defined as the differences in area between the loading/unloading curves, is represented by the shaded area of the hypothetical data.

3.6.3 Posterior Strut Deflection Analysis

The locations of the posterior strut markers for the latter five loading cycles for each test orientation were averaged and used to characterize strut deformation during loading. The mean total displacement in the sagittal plane between the pre-load and full load states was calculated for each marker and compared across loading orientations. The peak mean displacement (vector sum of the sagittal plane motion relative to the pre-load state) was calculated for each of the posterior strut active markers for each stance sub-phase and AFO.

3.6.4 Ankle Angle Analysis

The ankle angle sensor voltages for the latter five loading cycles were averaged. Both a 5^{th} order polynomial fit and spline fit calibration curves were used to determine mean ankle angles during loading. The ROM for the ankle was calculated for each stance sub-phase and AFO. Additionally, the maximum force corresponding to 5° ankle dorsiflexion relative to the pre-load position was noted for each condition and AFO. The 5° ankle dorsiflexion reference approximated the clinical "pain-free" ankle motion typically permitted by the IDEO for limb salvage patients.

3.6.5 Rotational Motion Analysis

The location of the proximal marker triads on the various AFOs at full load, relative to the corresponding pre-load locations, was analyzed for rotational motion (Figure 24). The mean angle of rotation, the average of vector rotation angles between triad marker pairs at full load, was determined to describe the rotational motion of the proximal AFO triad with respect to the testing coordinate system (Figure 13). Additionally, the rotations were determined using traditional Euler angle analysis. These results were contrasted with the vector rotation angle results. The corresponding centers of rotation of the proximal AFO triad (relative to fixed distal AFO marker

triads) were calculated for each stance sub-phase using a mean perpendicular bisector method: the intersections of the perpendicular bisectors of the motion vectors from the respective marker pairs were determined and averaged. The rotation of the triad at the toe of the AFO was not analyzed as the AFO toe region is essentially fixed to the loading plate during compressive pre-loading. The triad at the supramalleolar of the AFO may also move during loading, although such motion included motion in all three planes due to AFO deformation at the malleolar regions; the frontal and transverse plane motion was most pronounced for the thermoplastic AFO designs. The rotational motion of the supramalleolar triad was similarly determined for select AFO designs.

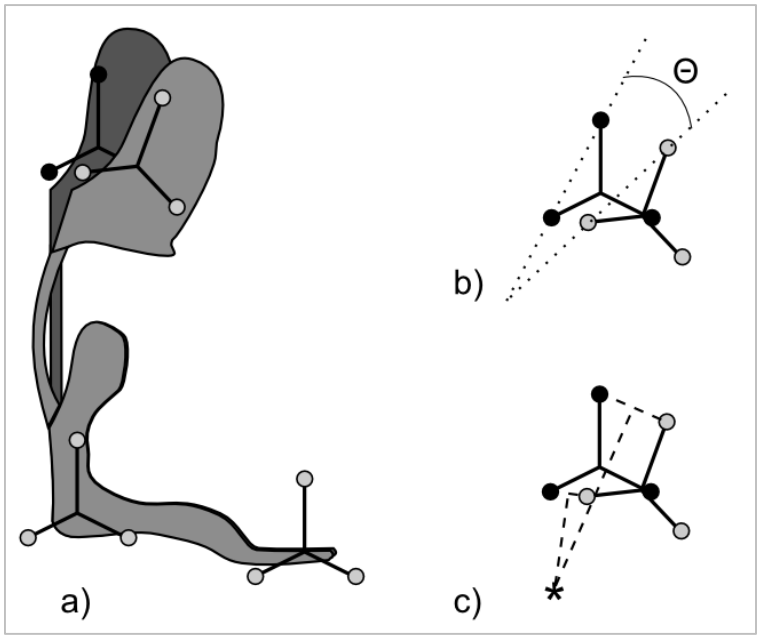

Figure 24: Rotational analysis using marker triads: a) triad locations at pre-load (black) and loaded states (grey), b) sample angle of rotation between marker position vectors, and c) sample center of rotation determined by the perpendicular bisector method.

3.6.6 Footplate Deformation Analysis

The footplates of the AFOs deformed with applied load. The deformation in the frontal plane was characterized based on the motion of the supramalleolar triad markers between the full load and pre-load states. The magnitude of the marker displacements were averaged over the

latter five loading cycles. The mean motion in the frontal plane was characterized by the superior-inferior and medial-lateral components. Medial-lateral deformation reflects “bulging”; superior-inferior deformation contributes to rotational motion in the sagittal plane.

3.6.7 Error Analysis

One potential source of error affecting the characterization of rotational motion is movement between the markers of each triad. The triads are assumed to be rigid bodies in the rotation calculations. Relative motion was quantified to determine error magnitude and the subsequent impact on rotational motion.

CHAPTER 4: RESULTS

The following chapter presents the results pertaining to the objectives of this study: 1) quantifying force-deflection curves and compressive stiffness of the tested AFOs, 2) quantifying the deflection of the posterior strut, and 3) characterizing the relative rotation of each AFO. For the purpose of this study the following terms are defined:

Motion:	all movement, translation and/or rotation, in any plane
Displacement:	translation in one plane defined by the global laboratory-based coordinate system
Deflection:	pattern of movement considering the motion relationship between multiple markers
Deformation:	motion out of the sagittal plane (motion in the frontal and/or transverse planes)

4.1 Force-Displacement Data

4.1.1 Loading Rate Independence

Representative mean force-displacement loading curves from preliminary cyclic loading at 5 mm/s and 10 mm/s for each AFO are presented in Figure 25. For the *displacement controlled* mechanical testing, the mean change in maximum load observed between loading rates was 1.1 (± 0.8) %. While the maximum applied displacement (corresponding to target load) varied across sub-phases and AFO designs, loading rate independence was consistently observed. As such, subsequent data analysis was conducted at 5 mm/s only, and the latter rotational motion studies were performed at 5 mm/s only.

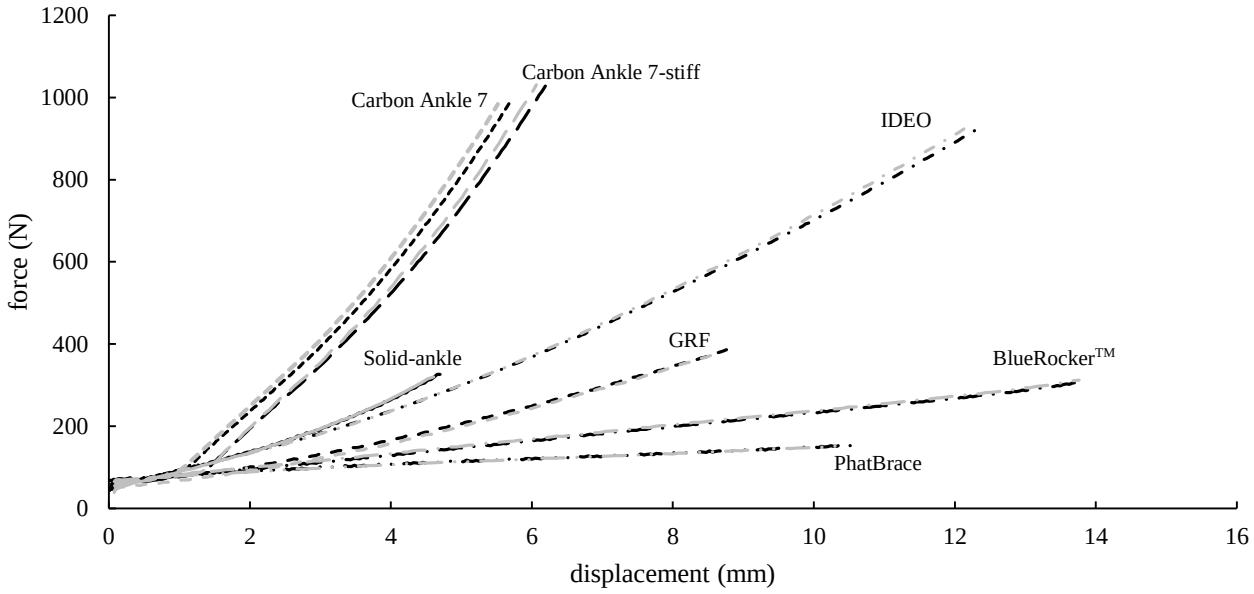

Figure 25: Mean force-displacement loading curves for cycles 6-10 for each AFO at MSt for both 5 mm/s (black) and 10 mm/s (grey) loading rates.

4.1.2 Preconditioning

To reduce potential preconditioning effects, data from the initial five cycles were excluded from analysis; only the latter five cycles were considered. These latter cycles were less variable (e.g., displacement corresponding to the target load was consistent) (Figure 26). A similar trend was observed for all AFOs at each tested sub-phase of stance. The decreased variability in the maximum displacement for the latter cycles relative to the initial cycles (Table 3) also demonstrate the reduced preconditioning effects.

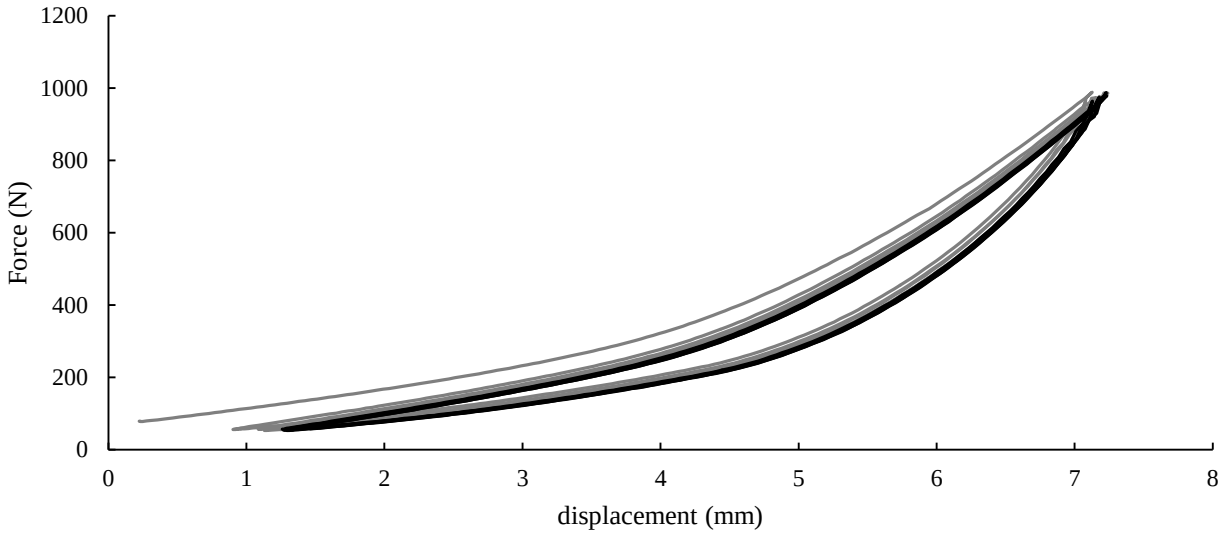

Figure 26: Force-displacement curves for the loading/unloading cycles 1-5 (grey) and cycles 6-10 (black) at 5 mm/s for the solid-ankle AFO at MSt.

Table 3: Comparison of variability in peak displacement for the initial and final five loading cycles at 5 mm/s for each AFO at MSt.

	Standard Deviation in Maximum Displacement (mm)	
	Cycles 1-5	Cycles 6-10
Solid-ankle	0.06	0.04
GRF	0.14	0.05
IDEO	0.21	0.13
PhatBrace	0.02	0.05

4.1.3 Hysteresis

Hysteresis, the difference in area under the loading/unloading portions of the force-displacement curves, was calculated to quantify energy lost between loading/unloading (Table 4). The area under the unloading portion has been reported as a potential measure of energy return for AFOs [35]. However, as the AFOs were unloaded at a controlled rate, as opposed to the quick

release observed during swing, this measure does not accurately characterize energy return and was not quantified.

Table 4: The total and normalized (with respect to the total area under the loading curve) hysteresis of the latter five loading cycles for each AFO at MSt for 5 mm/s trials. Data corresponding to partial loading trials are shown in grey.

	Hysteresis	
	Total (N-mm)	Normalized (%)
Solid-ankle	417 (± 7)	19.4 (± 0.3)
GRF	1414 (± 57)	19.1 (± 0.3)
IDEO	834 (± 3)	16.2 (± 0.1)
Carbon Ankle 7	632 (± 8)	26.5 (± 0.2)
Carbon ankle 7 – stiff	685 (± 8)	26.3 (± 0.2)
BlueRocker™	433 (± 2)	17.3 (± 0.1)
PhatBrace	514 (± 10)	18.2 (± 0.2)

4.1.4 Compressive Stiffness

To reduce potential error in ankle moment calculations due to AFO footplate compliance, variations in contact area and lever arm estimates, the peak displacement applied during preliminary compressive stiffness test procedure (see Section 3.6) was often less than the target displacement for the specific stance sub-phase. As such, the force-displacement and resultant final compressive stiffness of these partial loading trials are not representative of the mechanical behavior at the full target displacement. The force-displacement data for these partial loading trials are presented in Appendix C.

The compressive stiffness test procedure was repeated for full target load and orientation for each stance sub-phase for a subset of the AFOs (solid-ankle, GRF, IDEO, and PhatBrace). The resultant mean force-displacement data for cycles 6-10 at 5 mm/s are presented in Figure 27. For each AFO and stance sub-phase, displacement increases nonlinearly with increasing force.

The greatest displacement was observed during PSw loading, consistent with the dorsiflexed orientation and greater load magnitude for this sub-phase (see Table 2, Chapter 3).

During LR, the ankle plantar flexes to promote foot flat. AFOs may be prescribed to promote stability of the ankle, subtalar and knee joints during early stance. While the mechanical properties of the AFO-limb complex during early stance may be important, the focus of the current study is the potential energy return during late stance and the functional improvement during high energy tasks. Therefore only the results for the latter stance sub-phases are included in this chapter; the LR results are summarized in Appendix D.

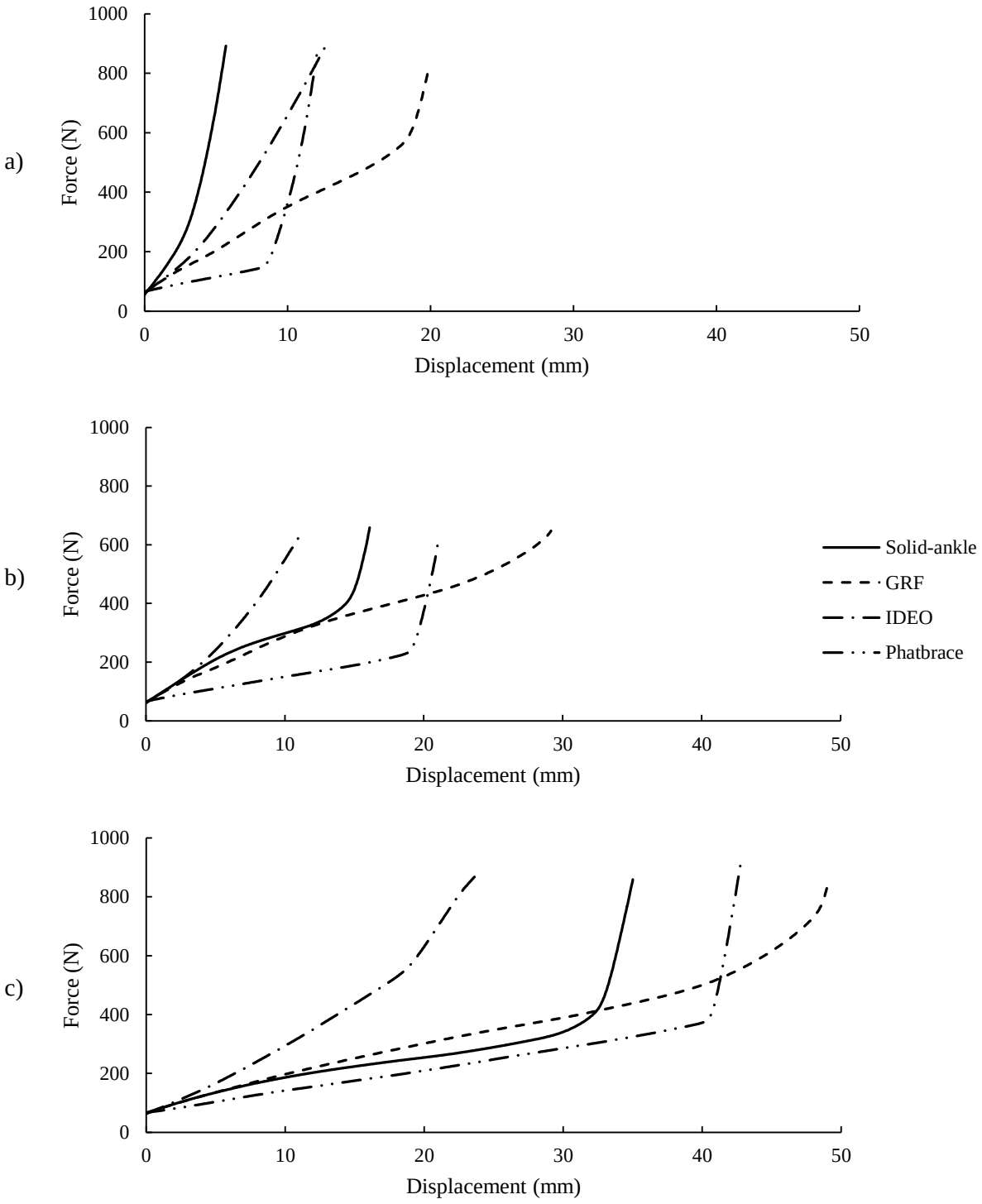

Figure 27: Mean force-displacement data across loading cycles 6-10 during compressive loading at 5 mm/s for a) MSt, b) TSt, and c) PSw sub-phases of stance. Target loads are noted (solid line) for each sub-phase of stance.

As detailed in Section 3.8.2, the compressive stiffness of the initial and final 25% of the loading curves was determined using linear regression. The initial compressive stiffness for both the partial and fully loaded trials (Figure 28) demonstrate decreased stiffness from MSt to PSw sub-phases of stance.

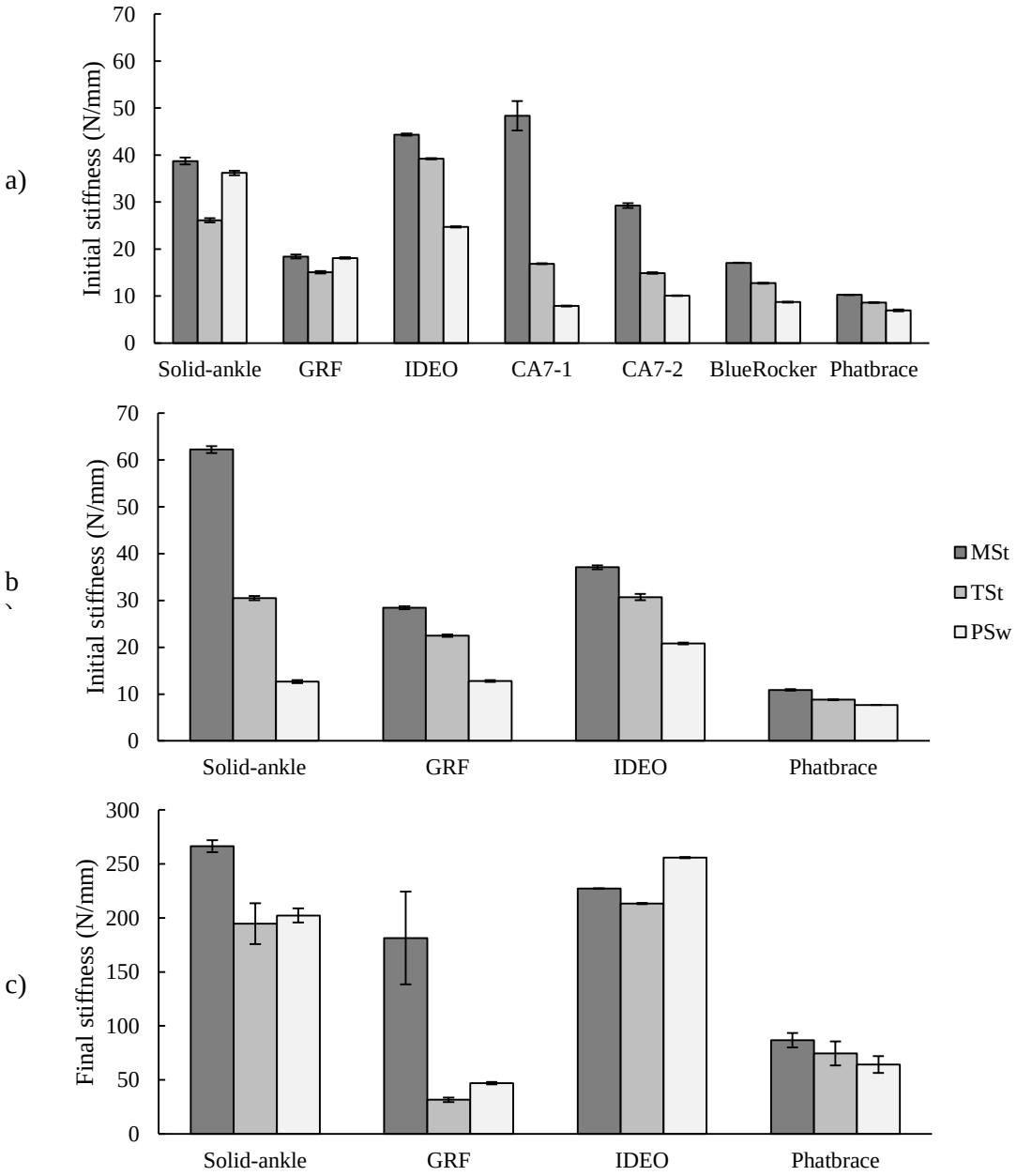

Figure 28: Initial compressive stiffness from a) partial loading trials and b) full loading trials for various AFOs during the latter sub-phases of stance; c) final compressive stiffness, full loading trials only, are also shown.

The final compressive stiffness exceed the initial stiffness for each AFO. No consistent trend in magnitude was observed between the stance sub-phases. Increased contact area between the plantar surface of the AFO and the footplate was observed for some AFOs, particularly the thermoplastic designs. The compressive stiffness transitioned from the more compliant initial stiffness to the less compliant final stiffness when full contact of the plantar surface was achieved (Figure 27).

4.2 Strut Deflection

The maximum deflection of the posterior strut of each AFO during loading was characterized using motion analysis. Maximum displacements in the sagittal plane at the final target load are summarized in Table 5 for the latter stance sub-phases. The IDEO demonstrated greater strut displacement than the other AFOs for all latter stance sub-phases. The corresponding peak loads applied during the partial and full target loading trials are contrasted in Table 6.

Table 5: Maximum sagittal plane strut displacement from pre-load to full load at various sub-phases of stance. The location of maximum displacement is noted as proximal (P), mid- (M), or distal (D) third of the strut region. Data corresponding to the partial loading trials are shown in grey.

	Maximum Strut Displacement (mm)					
	MSt		TSt		PSw	
Solid-ankle	2.10 (± 0.01)	P	2.80 (± 0.01)	P	2.02 (± 0.01)	P
GRF	2.70 (± 0.01)	M	3.92 (± 0.01)	M	2.53 (± 0.02)	M
IDEO	9.07 (± 0.02)	M	8.21 (± 0.02)	M	12.88 (± 0.01)	M
Carbon Ankle 7	3.97 (± 0.01)	P	2.36 (± 0.01)	D	6.63 (± 0.01)	D
Carbon Ankle 7 - stiff	4.04 (± 0.02)	P	2.92 (± 0.02)	P	4.07 (± 0.02)	D
BlueRocker™	5.88 (± 0.01)	M	5.40 (± 0.02)	M	4.94 (± 0.01)	M
PhatBrace	3.43 (± 0.01)	M	4.73 (± 0.01)	M	3.48 (± 0.01)	M

Table 6: Peak loads applied during partial (grey) and full loading trials.

	Maximum Load (N)		
	MSt	TSt	PSw
Solid-ankle	328 (± 2)	316 (± 3)	299 (± 4)
GRF	387 (± 3)	294 (±1)	293 (± 3)
IDEO	923 (± 2)	721 (± 1)	871(± 2)
Carbon Ankle 7	997 (± 6)	369 (± 3)	326 (± 3)
Carbon Ankle 7 – stiff	1034 (± 4)	791 (± 4)	227 (± 3)
BlueRocker™	312 (± 1)	269 (± 1)	231 (± 3)
PhatBrace	154 (± 1)	163 (± 2)	154 (± 1)
Target	880.7	640.5	880.7

The location along the posterior strut where maximum displacement occurred differed between AFO designs, as noted in Table 5. The strut displacement at each marker location along the strut are plotted in Figures 29-31 for the latter sub-phases of stance, comparing the final deflected AFO strut to the pre-loaded strut position. To improve understanding of the deflection mechanism, the displacement magnitude at the final load, full or partial, for all markers along the posterior strut are plotted in Figure 32.

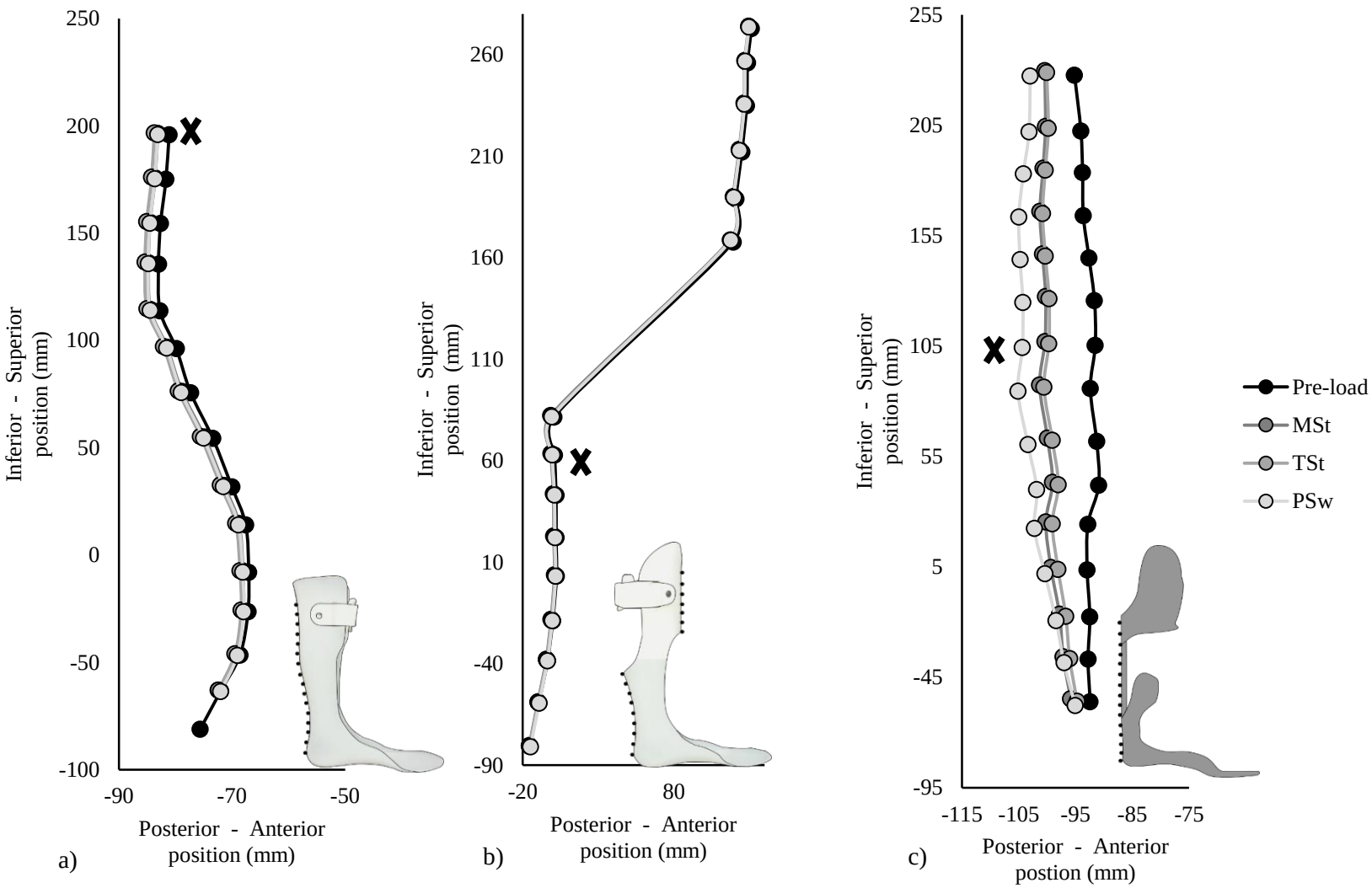

Figure 29: Position of posterior strut markers at pre-load and full load for the various sub-phases of stance for the a) solid-ankle, b) GRF, c) IDEO AFO. The solid-ankle and GRF AFOs were partially loaded for each sub-phase of stance. The location corresponding to maximum displacement is noted with X. For reference, the marker locations on each AFO are included.

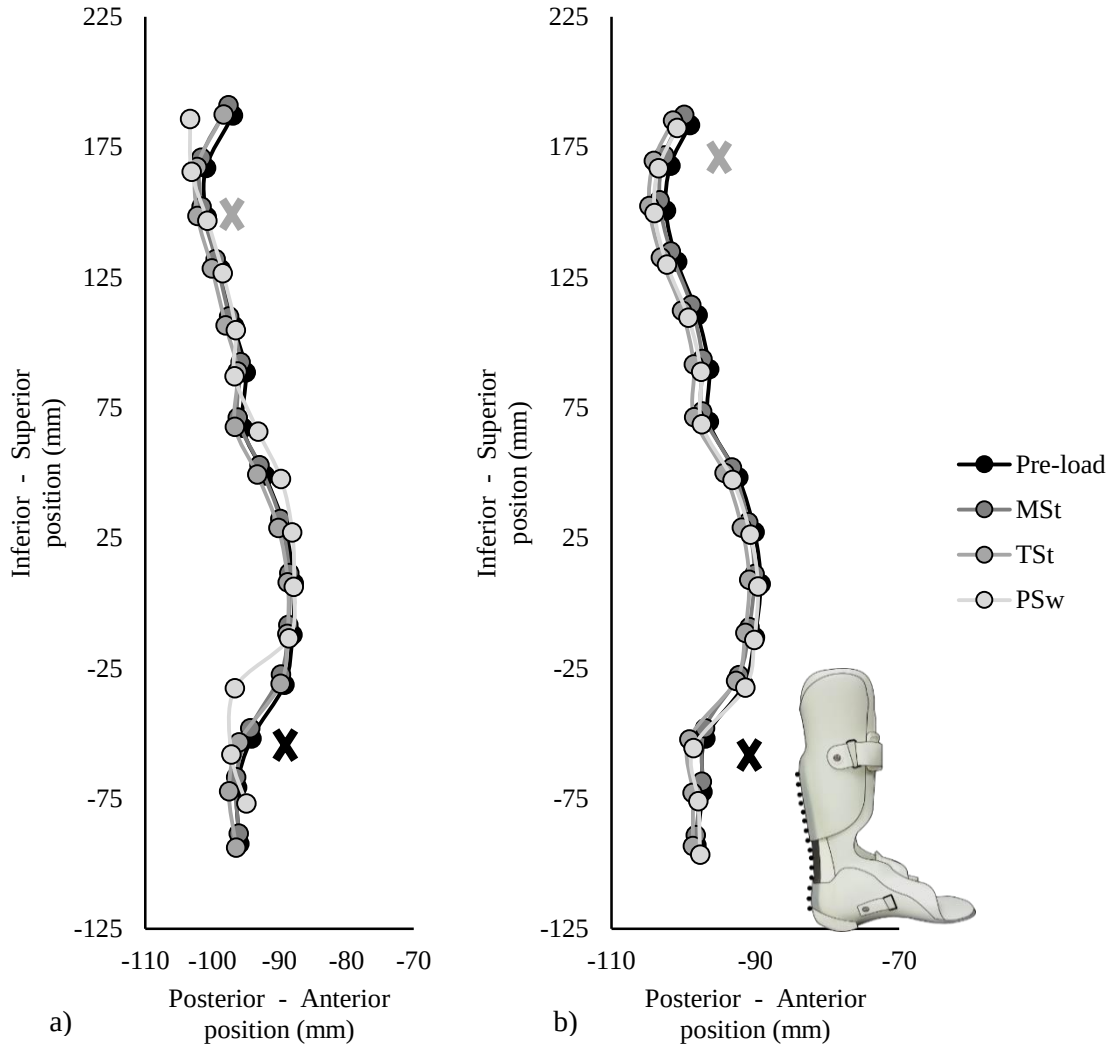

Figure 30: Position of posterior strut markers at pre-load and full load of the various sub-phases of stance for the CA7 AFO: a) normal and b) stiff struts. The normal and stiff CA7 AFOs were partially during PSw testing. The location corresponding to the maximum displacement is noted with X (grey: at MSt and TSt, black: at PSw). For reference, the marker locations on each AFO are included.

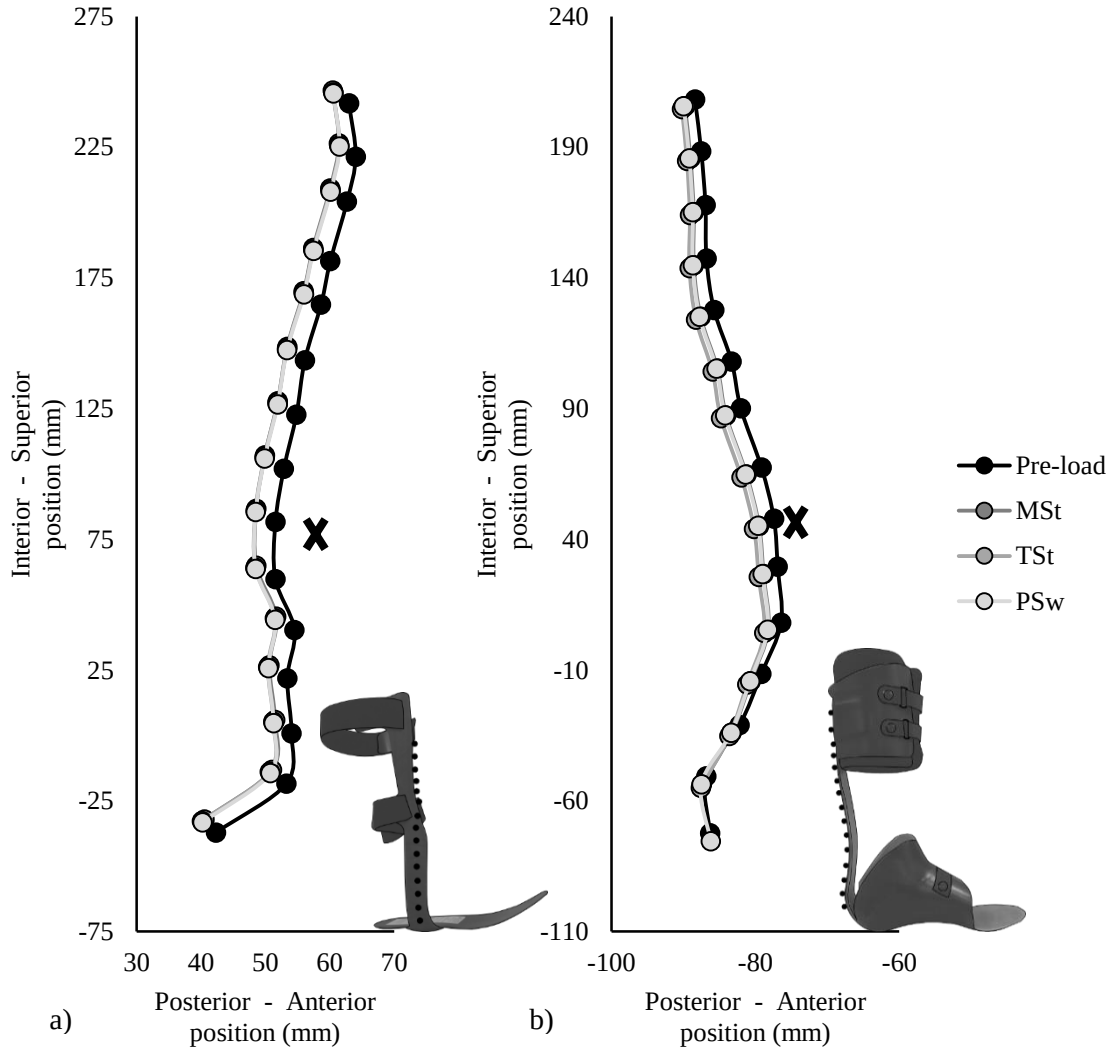

Figure 31: Position of posterior strut markers at pre-load and full load for the various sub-phases of stance for the a) BlueRocker™ and b) PhatBrace AFOs. The BlueRocker™ and PhatBrace AFOs were partially loaded for each sub-phase of stance. The location corresponding to maximum displacement is noted with X. For reference, the marker locations on each AFO are included.

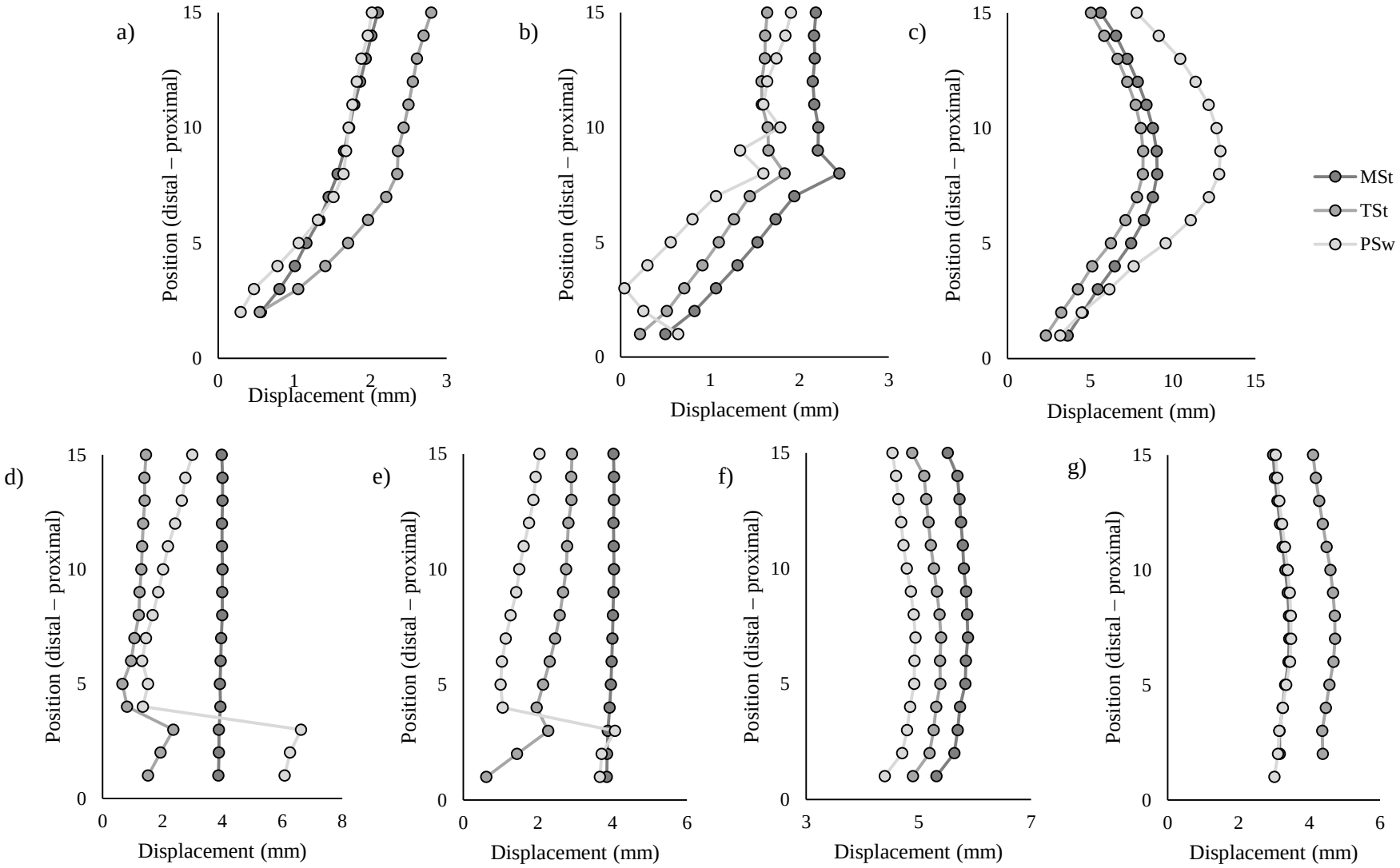

Figure 32: Sagittal displacement of posterior strut markers at final load at various sub-phases of stance at AFOs: a) solid-ankle, b) GRF, c) IDEO, d) Carbon Ankle 7 – normal, e) Carbon Ankle 7 – stiff, f) BlueRocker™, and g) PhatBrace. As previously noted, AFOs were subjected to varying final loads (Table 6).

4.3 Rotational Analysis

4.3.1 Surrogate Limb Ankle Rotation

The inductive ankle sensor was used to quantify the rotation of the surrogate limb ankle during compressive loading to the full target loads for the latter stance sub-phases. The respective ankle ROM during loading (Table 7), as well as the maximum force corresponding to 5° ankle ROM (Table 8), were measured for a subset of AFOs. For the IDEO, the ankle ROM was less than 6.1° for all sub-phases of stance. The maximum force corresponding to 5° ankle dorsiflexion was greatest for the IDEO for all stance sub-phases.

Table 7: Average surrogate ankle ROM for various AFOs during late stance. Results from both calibration curves, 5th order polynomial and spline, are included.

	Ankle ROM (°)					
	Polynomial Calibration			Spline Calibration		
	MSt	TSt	PSw	MSt	TSt	PSw
Solid-ankle	3.04 (± 0.08)	8.22 (± 0.09)	12.18 (± 0.09)	2.91 (± 0.09)	8.42 (± 0.09)	10.97 (± 0.12)
GRF	10.26 (± 0.19)	13.57 (± 0.05)	18.58 (± 0.13)	10.54 (± 0.19)	14.07 (± 0.05)	17.42 (± 0.18)
IDEO	4.49 (± 0.09)	3.39 (± 0.16)	5.77 (± 0.11)	4.13 (± 0.10)	2.94 (± 0.15)	6.09 (± 0.14)
PhatBrace	7.45 (± 0.11)	10.60 (± 0.11)	13.36 (± 0.09)	7.27 (± 0.12)	10.69 (± 0.10)	12.39 (± 0.10)

Table 8: The average observed force at 5° ankle dorsiflexion for various AFOs during late stance. Results from both calibration curves, 5th order polynomial and spline, are included. For trials in grey, the full target load resulted in less than 5° ankle dorsiflexion.

	Force at 5° Ankle Dorsiflexion (N)					
	Polynomial Calibration			Spline Calibration		
	MSt	TSt	PSw	MSt	TSt	PSw
Solid-ankle	900 (± 57)	301 (± 7)	213 (± 5)	804 (± 49)	299 (± 7)	208 (± 4)
GRF	402 (± 4)	336 (± 5)	221 (± 3)	371 (± 4)	317 (± 6)	233 (± 2)
IDEO	907 (± 3)	648 (± 15)	725 (± 46)	854 (± 12)	615 (± 17)	740 (± 30)
PhatBrace	147 (± 2)	142 (± 2)	171 (± 3)	211 (± 13)	148 (± 2)	166 (± 3)

4.3.2 AFO Rotation

The mean sagittal rotation of the proximal triad on the AFO relative to the global laboratory-based coordinate system for full loading during the latter phases of stance is summarized in Table 9. The IDEO demonstrated the greatest rotation at full target load for all sub-phases of stance tested. As described in Section 3.8.5, three sagittal centers of rotation were also determined for each trial, based on the change between the initial and final positions of each pair of proximal triad markers. The distances between the calculated centers of rotation and the proximal triad of each AFO (Figure 33) were highly variable with large standard deviations (Table 10).

Table 9: Average rotation of the proximal triad in the global coordinate system, determined by both vector and Euler analysis, for various AFOs during late stance.

	Proximal AFO Rotation (°)					
	Vector Analysis			Euler Analysis		
	MSt	TSt	PSw	MSt	TSt	PSw
Solid-ankle	0.03 (± 0.02)	0.20 (± 0.01)	0.80 (± 0.07)	0.03 (± 0.00)	0.18 (± 0.01)	0.81 (± 0.01)
GRF	0.61 (± 0.27)	0.66 (± 0.31)	0.66 (± 0.78)	1.09 (± 0.01)	1.87 (± 0.01)	3.65 (± 0.02)
IDEO	2.16 (± 0.17)	1.64 (± 0.09)	2.45 (± 0.17)	2.27 (± 0.03)	1.82 (± 0.03)	2.91 (± 0.01)
PhatBrace	0.86 (± 0.01)	0.14 (± 0.03)	0.45 (± 0.07)	0.85 (± 0.05)	0.14 (± 0.07)	0.43 (± 0.05)

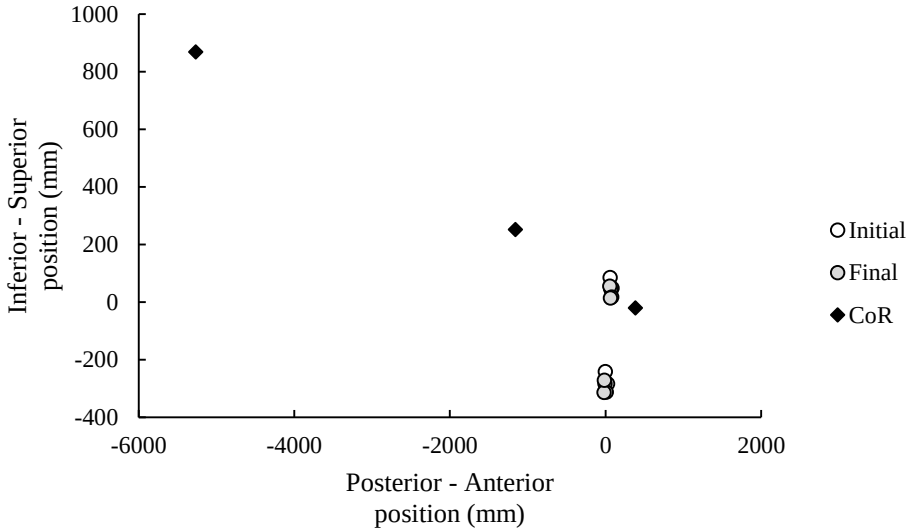

Figure 33: The calculated centers of rotation for the GRF AFO at TSt. The distances from each center of rotation to the final anterior proximal marker were used to quantify the variability between calculations. The initial and final proximal and supramalleolar marker positioned are plotted for reference.

Table 10: AFO centers of rotation (mean and standard deviation) relative to the origin of the initial proximal triad during late stance.

	Relative Center of Rotation (mm)		
	MSt	TSt	PSw
Solid-ankle	18083 (± 20110)	5692 (± 817)	3532 (± 974)
GRF	1426 (± 1679)	2323 (± 2705)	7011 (± 5800)
IDEO	770 (± 17)	11141 (± 6845)	9135 (± 6489)
PhatBrace	750 (± 683)	498 (±110)	652 (± 132)

4.3.3 Footplate Deformation

As previously noted, loading to the full target load caused some AFO designs to deform in the malleolar region such that full contact occurred between the AFO plantar surface and the loading plate (Figure 34). These malleolar deformations of the AFOs precluded analysis of supramalleolar marker triad rotation (Figure 35). To characterize the deformation of the

malleolar region of the AFO, the medial/lateral and superior/inferior components of the frontal plane motion of the supramalleolar triad were quantified (Figure 36). The greatest medial-lateral displacement in the frontal plane at the malleolar region (8-22%) was observed for the thermoplastic AFOs (solid-ankle and GRF AFOs); the medial-lateral displacement at the malleolar region of the AFO was greatly reduced for the carbon fiber designs (IDEO and PhatBrace). The frontal and coronal plane deformations of the malleolar region of AFOs may introduce sagittal plane analysis errors, depending on the location of the supramalleolar triad. For example, a 30° rotation in the frontal plane or the coronal plane may introduce errors of approximately 6 mm and 16 mm, respectively, in the sagittal displacement, the plane of interest in this study.

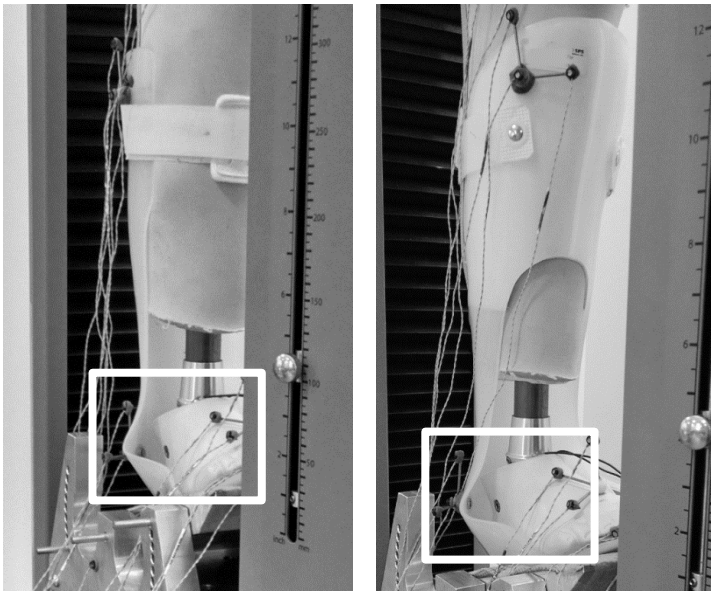

a) b)

Figure 34: Deformation of malleolar region of the a) solid-ankle, and b) GRF AFOs contributing to full contact of the plantar surface of the AFO with the loading plate.

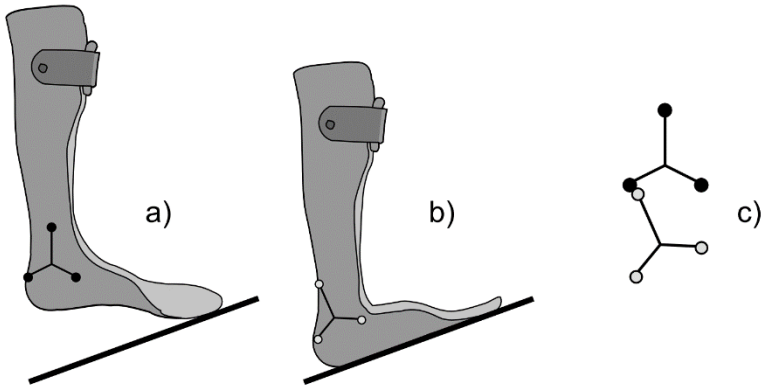

Figure 35: The pre-load a) and final positions, b) of the supramalleolar triad during PSw testing. The pre-load and final positions superposed in c) illustrate the magnitude of superior-inferior motion observed during testing.

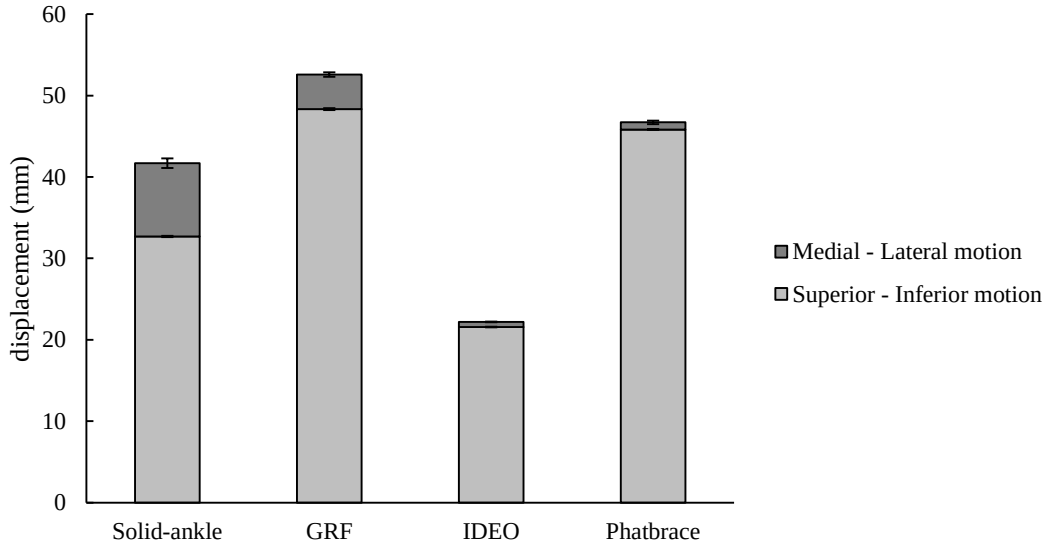

Figure 36: Maximum frontal plane motion of the supramalleolar triad during PSw loading trials to the full target load. The overall motion is divided into the peak medial-lateral and superior-inferior components.

To further characterize the motion and/or deformation of the AFO footplate, the mean rotation of the supramalleolar triad in the sagittal plane, relative to the global coordinate system was determined for each sub-phase (Table 11). Due to the potential errors in sagittal position from out of plane motion, only the IDEO and PhatBrace AFO were considered. The PhatBrace

demonstrated greater rotation of the supramalleolar region through TSt and PSw. The rotation of the IDEO supramalleolar triad was less than 5° for all sub-phases of stance.

Table 11: Average rotation of supramalleolar triad in the sagittal plane (global coordinate system) for two AFOs during sub-phases of stance.

	Supramalleolar Rotation (°)					
	Vector Analysis			Euler Analysis		
	MSt	TSt	PSw	MSt	TSt	PSw
PhatBrace	3.12 (± 0.11)	6.80 (± 0.09)	13.65 (± 0.58)	3.20 (± 0.04)	6.83 (± 0.06)	18.41 (± 1.33)
IDEO	3.20 (± 0.03)	2.41 (± 0.02)	4.63 (± 0.03)	3.22 (± 0.05)	2.39 (± 0.04)	4.55 (± 0.01)

4.4 Summary

The mechanical properties of compressive stiffness, strut deflection, and proximal and distal AFO rotation, as well as the rotation of the ankle of the underlying surrogate limb, were evaluated for several AFO designs. Traditional thermoplastic (solid-ankle and GRF) and carbon fiber (PhatBrace) AFO designs demonstrated greater frontal plane motion at the malleolar region that resulted in full contact of the plantar surface with the loading plate. These designs were characterized by small strut deflection and proximal rotational, as well as large surrogate limb ankle ROM. In contrast, the mechanical response of the IDEO was unique, demonstrating large deflection along the posterior strut, minimal frontal plane deformation in the malleolar region, greater proximal rotation, and minimal surrogate limb ankle ROM.

CHAPTER 5: DISCUSSION

The results of the compressive stiffness, strut deflection, and rotational motion of the tested AFOs are discussed, specifically concerning the research objectives: 1) to quantify force-deflection curves and characterize the compressive stiffness of the tested AFO designs, 2) to quantify the deflection of the posterior strut, and 3) to characterize the rotation of the proximal and distal segments of each AFO. The results of the IDEO are compared to alternative AFO designs in the context of the hypotheses: the deflection mechanism of AFOs under load will differ between designs, and the IDEO will demonstrate greater deflection throughout the posterior strut and greater rotational movement of the proximal and distal segments of the AFO. The key findings of the study are reviewed, discussing the related clinical impact. Limitations of this study are presented and modifications are proposed for future studies. Finally, suggestions for future AFO designs and AFO prescription are summarized.

5.1 Force-Displacement

5.1.1 Loading Rate Independence

The mechanical loading behavior, including loading rate dependence, of the IDEO has not been previously characterized. For each AFO and stance sub-phase, the relationship between vertical displacement and force was independent of loading rate (1.1± 0.8% mean change in peak load) over the range of 5-10 mm/s (Figure 25, Chapter 4), confirming the observations of Yamamoto et al. [25]. The loading rate independence of many AFO designs support prior mechanical bench testing protocols conducted at a single loading rate. Loading rates ranged from 0.5 – 50 °/s for rotation controlled studies [25, 28, 33], 0.169 - 200 mm/s for displacement controlled studies [29, 30], and 100-250 N/sec for force controlled studies [34, 36]. Several studies, however, conducted mechanical testing of AFOs by applying displacements manually

(Table 1, Chapter 2) such that the loading rate was not controlled; the potential dependence of mechanical properties for such test conditions is not known. Potential loading rate dependence for rates beyond the range tested in this study, as relevant to higher activity tasks, require further testing. Regardless of potential rate dependence, displacement, deflection, rotation, [28, 33], or compressive force [29, 30] should be applied at controlled, clinically relevant rates for consistent results.

5.1.2 Preconditioning

The AFOs were mechanically tested using cyclical compressive loading. Data from the initial cycles were excluded from analysis to reduce potential preconditioning effects. The decreased mean variability in the maximum displacement in latter cycles (0.04-0.13 mm) compared to the initial cycles (0.02-0.21 mm) indicates that preconditioning is necessary. While previous AFO studies have performed multiple loading/unloading cycles, few excluded initial cyclic data [29, 33], preconditioning effects have not previously been characterized. If not considered, preconditioning effects may affect force-displacement and/or moment-rotation data, contributing to variation in compressive and rotational stiffness calculations.

5.1.3 Hysteresis

Hysteresis was quantified in this study to characterize energy lost during compressive loading/unloading (Table 4, Chapter 4). The normalized hysteresis of the IDEO (16.2%) was less than other AFO designs (17.3-26.5%) during MSt, suggesting that potentially less energy is lost during loading/unloading with this AFO. However, the clinical relevance of these hysteresis measures is limited. The AFOs tested during this study were unloaded at a controlled rate. More clinically relevant testing might characterize the energy return of the AFO at the transition from stance to swing; such testing would require quick unloading or load release, such as that observed

during gait. While the presented hysteresis results have limited clinical relevance, a difference in the energy storage/release between the IDEO and traditional AFO designs appears to exist. Future studies involving mechanical testing of AFOs might include dynamic unloading to further quantify and characterize energy storage/release mechanisms.

5.1.4 Compressive Stiffness

For each AFO, the resultant displacement increased nonlinearly with increasing force; the displacement at the respective target load for each sub-phase of stance increased from early to late stance, with the largest displacement occurring during PSw (Figure 27, Chapter 4). For the solid-ankle and PhatBrace AFOs, the transition from initial to final stiffness was abrupt; these stiffness transitions were more gradual for the IDEO and GRF AFOs. The abrupt transition to increased stiffness may be attributed to the increased contact area between the plantar surface of the solid-ankle and PhatBrace AFOs and the loading plate with increased load. While the GRF experienced similar deformation and increased contact area, the transition from initial to final stiffness was less abrupt with this AFO, perhaps due to the AFO design characteristics or the poor fit of the GRF AFO on the surrogate limb.

The initial compressive stiffness values have little clinical relevance as AFOs are quickly brought to full load during gait; the final compressive stiffness at the full target load for the various stance sub-phases has more relevance to gait. However, the initial stiffness may be used to categorize AFOs. For example, the solid-ankle AFO and the IDEO can be categorized as stiff AFOs, with high initial stiffness for all sub-phases of stance. In contrast, the BlueRocker™ and PhatBrace AFOs are flexible, with low initial stiffness for all sub-phases of stance. AFOs, however, have been more commonly categorized based on their fabrication material (thermoplastic or carbon fiber), trimlines (supramalleolar), or design features (articulated versus non-articulated).

The more clinically relevant final compressive stiffness exceeded the initial stiffness values for each AFO (Figure 27, Chapter 4), but demonstrated no consistent trend in stiffness with stance sub-phase. As mentioned previously, the transition from the more compliant initial stiffness to the less compliant final stiffness occurred at the onset of full contact between the AFO plantar surface and the loading plate for the thermoplastic and PhatBrace designs. The final compressive stiffness for the solid-ankle AFO and IDEO appear dependent on target load magnitude, with greater final stiffness observed for MSt and PSw for which greater target loads were applied (880.7 N for MSt and PSw; 640.5 N for TSt). However, since full contact between the AFO and the ground is not clinically observed, these final compressive stiffness values are artificially high.

Based on the measured initial and final compressive stiffness, the IDEO exhibited similar mechanical characteristics to the solid-ankle AFO. While the prescription criteria for these AFOs overlap (Section 2.2), the resultant functional performances differ greatly (Section 2.2). As such, compressive stiffness alone does not fully describe the AFOs' mechanical behavior.

Only one other study characterized the mechanical behavior of a carbon-fiber posterior leaf spring AFO with force-displacement data [30]. The final compressive stiffness measured by Hawkins (~8-41 N/mm) is comparable to the initial compressive stiffness determined in the present study (7-48 N/mm) [30]. However, Hawkins' values for a carbon-fiber AFO are more compliant than the final compressive stiffness measured in the current study for thermoplastic and carbon-fiber AFOs (64-87 N/mm). This difference may be attributed to variations in the mechanical testing protocol designs and AFOs tested. In Hawkins's study, a 100-150 N load was applied at 1.69 mm/min (target peak load or displacement was not specified) to the carbon-fiber posterior leaf spring AFO (without a surrogate limb) as pure compression between two platens.

The AFO footplate was fixed to one platen with the strut initially oriented perpendicular to the platens and the proximal contact point was allowed to slide along the top platen [30]. The peak load applied to the AFOs in the current study was 880.7 N; for initial stiffness calculations, peak loads of 100-200 N were applied. The increased load magnitude and alternative AFO materials and designs likely attributed to the observed variations in final AFO compressive stiffness between these studies.

5.2 Strut Deflection

In addition to quantifying AFO stiffness, this study also measured AFO strut deflection. The maximum displacement of the posterior strut of the IDEO (8.2 to 12.9 mm) exceeded that for the other AFOs (3.7 to 4.0 mm) for all latter stance sub-phases. The maximum strut displacement occurred mid-strut, as seen in Figure 29 (Chapter 4). Relative to the pre-load strut position, the IDEO demonstrated a deflection pattern similar to a column subjected to compressive loading, buckling at mid-strut. This deflection mechanism is confirmed by the displacement of the strut markers from the pre-load to full target load states (Figure 32, Chapter 4); the displacement curve increases then decreases moving proximally to distally, with the apex at mid-strut.

The mechanism for posterior strut deflection can also be reviewed for the other study AFOs. For many of these designs, however, the AFOs were not tested to the full target load. As such, comparison of maximum strut displacement between partial and full target loaded states is inconclusive. Qualitative analysis of the displacement of each posterior strut marker, however may still provide insight regarding the method of strut deflection of each AFO. The displacement curves of the strut markers in the sagittal plane in Figure 32 (Chapter 4) show different patterns of deflection. Increased relative anterior-posterior displacement along the strut, proximally or distally, reflects sagittal plane rotation. The solid-ankle and GRF AFOs demonstrated increased

anterior-posterior displacement of the distal posterior strut markers, with reduced anterior-posterior displacement proximally. Both Carbon Ankle 7 designs exhibited a similar trend during TSt and PSw loading. The thermoplastic ankle-footplate of the Carbon Ankle 7 design appeared to rotate independently of the carbon fiber strut, contributing to large anterior-posterior displacement of markers at the thermoplastic heel. The minor anterior-posterior displacement of the posterior strut markers suggests that this region of the AFO is stiff, limiting deflection throughout the device or forcing deflection and/or deformation to occur elsewhere. The BlueRocker™ showed displacements corresponding to column buckling, but to a lesser magnitude than for the IDEO and PhatBrace AFO, with the maximum anterior-posterior displacement occurring at the mid-strut. The PhatBrace AFO, another carbon-fiber design, demonstrated large anterior-posterior displacements mid-strut and column buckling similar to that of the IDEO. Further testing to the full target load is needed to confirm these deflection mechanisms with increased load magnitude.

The deflection mechanism of the carbon fiber designs, particularly the IDEO and PhatBrace AFO, differ from those of the traditional thermoplastic designs. The mid-strut buckling deflection may contribute to enhanced energy storage during stance and energy release during swing. Further testing is needed to fully characterize the efficiency and mechanism of energy storage in the tested AFO designs.

5.3 Rotational Analysis

5.3.1 Ankle Sensor Calibration

Regression of the ankle angle sensor calibration curves to a fifth order polynomial (Equation 1, Chapter 4) captured the observed nonlinearity of the inductive sensor output. This regression resulted in maximum errors of 1.8° and 1.0° at 11° and 1° ankle plantar flexion,

respectively (Figure 21, Chapter 3). The ankle angle sensor calibration was also fit to a spline, resulting in a maximum error of 1.5º at 3º plantar flexion (Figure 38, Appendix B). During AFO testing, the range of motion of the ankle of the surrogate limb was 0-20° dorsiflexion for the solid-ankle and PhatBrace AFOs, and 3-9° plantar flexion for the IDEO. The maximum sensor regression error for both curve fits and both ranges of ankle motion was 1.5°. Ankle sensor errors may have contributed to greater reduction in peak force estimates at 5° ankle dorsiflexion.

5.3.2 Surrogate Limb Ankle Rotation

The ankle ROM of the traditional AFO designs (solid-ankle, GRF, and PhatBrace AFOs) increased from MSt to PSw, corresponding to the increased dorsiflexed orientation via the loading plate (Table 7, Chapter 4). Similar trends were observed in both the polynomial and spline analyses. As the plantar surface of the AFOs come into full contact with the loading plate, the ankle of the surrogate limb rotates. For the IDEO, ankle ROM was less than 6.1° for all sub-phases of stance. Limb salvage patients reduced ankle mobility due to ankle fusion and/or nerve damage of the surrounding tissue; for many, their "pain-free" range of ankle motion is less than 5° [37]. For the AFOs tested, only the ankle ROM of the surrogate limb with the IDEO was restricted to a clinically acceptable range for this patient population. As such, these alternative AFOs would not provide sufficient motion constraint to protect the potentially painful ankle.

The peak force corresponding to 5° ankle dorsiflexion was greatest for the IDEO for all stance sub-phases (IDEO: 615 to 907 N). The PhatBrace AFO demonstrated the smallest peak force (142 to 211 N) for all stance sub-phases, while the solid-ankle and GRF AFOs demonstrated marginally greater forces (213 to 402 N) with the exception of the solid-ankle at MSt (900 N). Again, while final values differed between the polynomial and spline analyses, similar trends were observed. The larger peak force observed with the IDEO may indicates that

the IDEO provides improved structural support, reducing the compressive load on the ankle and enhancing protection of the joint.

5.3.3 AFO Rotation

The IDEO demonstrated the greatest rotation of the proximal triad (2.5± 0.2° at PSw, see Table 9, Chapter 4 for all values) during testing at the full target load of all stance sub-phases. With the exception of the GRF AFO, the AFO rotation was similar using both vector and Euler analysis methods; for the GRF AFO, AFO rotation was 78 to 453% higher with the Euler analysis method. The enhanced proximal rotation observed with the IDEO further supports the aforementioned finding that the deflection mechanism of the IDEO strut differs from that of the other study AFOs, confirming the research hypotheses. For limb-salvage patients, more proximal AFO rotation likely minimizes the rotational demand of the patient's potentially painful and/or fused ankle joint, thereby confirming prescription criteria for the IDEO.

While the rotation of the proximal triad can be used to infer the orthotic center of rotation, estimation of the specific center of rotation using the perpendicular bisector method resulted in large standards of deviations (Table 10, Chapter 4) and little confidence in this measure. The variability may be attributed, at least in part, to the small magnitude of rotation observed and the efficacy of the perpendicular bisector method. These inaccuracies in the estimation of the orthotic center of rotation, however, did not affect the calculated proximal rotation magnitudes. To improve the accuracy in the estimation of the centers of rotation, more robust methods (e.g., least squares solutions [38]) of calculation might be implemented. Reliable centers of rotation estimates may provide insight regarding the ankle rotation permitted by the AFO. For example, a center of rotation near the ankle center would suggest greater ankle rotation relative to an AFO with a center of rotation offset from the ankle center.

5.3.4 Footplate Deformation

The thermoplastic AFO designs, specifically the solid-ankle and GRF AFOs, deformed at the malleolar region as the AFO plantar surface made full contact with the loading plate. The observed bulging in the malleolar region contributed to medial-lateral motion of the supramalleolar marker triad in the frontal and transverse planes (Figure 36, Chapter 4). As such, analysis of the supramalleolar triad motion in the sagittal plane was not conducted for the thermoplastic AFOs.

The frontal plane motion of the supramalleolar marker triads for the PhatBrace and IDEOs was primarily composed of superior-inferior displacement (Figure 36, Chapter 4), implying that these AFO footplates undergo motion primarily in the sagittal plane. The PhatBrace demonstrated greater sagittal plane rotation of the supramalleolar marker triad (13.7 ± 0.6° at PSw, see Table 11, Chapter 4 for all values), for both vector and Euler angle analysis, that contributed to the increased contact area between the AFO plantar surface and the loading plate. The modest sagittal plane rotation of the supramalleolar triad on the IDEO (4.6 ± 0.03° at PSw) was not sufficient to bring the IDEO footplate into full contact with the loading plate during testing. The lack of deformation and rotation of the IDEO footplate and supramalleolar region, respectively, suggest that these sections of the device remains rigid, permitting only slight rotation in the sagittal plane, similar to the proximal section of the IDEO. The reduced sagittal plane rotation of the IDEO's supramalleolar region assists in protecting the ankle and subtalar joints by limiting rotational motion.

5.4 Key Findings

For lower limb salvage patients, the IDEO has facilitated improved functional outcomes clinically in terms of temporal-spatial parameters (e.g., walking speed, cadence, step and stride

length) and energy cost [11]. However, the mechanical behavior of the IDEO, compared to traditional thermoplastic and carbon fiber AFO designs, is poorly understood. A review of mechanical AFO testing techniques, sensors, and designs was presented; results pertaining to the design of orthotic testing protocols were identified. In this study, the mechanical characteristics of compressive stiffness, strut deformation, and rotation of AFO regions were examined as research objectives. It was hypothesized that the IDEO will demonstrate a unique method of posterior strut deflection with a greater magnitude of displacement, as well as greater rotational movement of the proximal and distal segments of the orthosis. The rotation of the enclosed ankle was also investigated to contrast the AFOs in the context of prescription for the typical IDEO target patient population, limb salvage patients.

The key findings of this study, and the associated clinical impacts, are summarized below.

1. The force-displacement results of the tested AFOs demonstrated rate independence over a 5-10 mm/s compressive displacement rate range. Modest preconditioning was observed.
    - Investigators interested in characterizing and/or quantifying the mechanical properties of AFOs should be aware of limitations inherent with the testing protocol design. For consistent, clinically relevant results, mechanical testing should be conducted at a single loading rate (relevant to the task of interest). Multiple cycles of loading/unloading should be performed with the initial 1-5 cycles excluded from analysis to minimize potential preconditioning effects.

2. The normalized hysteresis between loading/unloading force-displacement curves was reduced in the IDEO.
    - The reduced hysteresis observed with the IDEO, relative to traditional AFOs suggests that there may be a difference in energy lost, and perhaps energy storage/release, between designs.

- Investigation of energy return of AFOs should include dynamic unloading or quick load release to quantify and characterize energy storage/release mechanisms, relevant to the behavior of AFOs at the transition from stance to swing during ambulation.

3. The IDEO and solid-ankle AFO exhibited similar final compressive stiffness.
   - The clinical prescription criteria for the IDEO and the solid-ankle AFO overlap, though the functional performance of each differ. Their comparable final compressive stiffness indicates that this mechanical property alone does not fully characterize an AFO's mechanical behavior.

4. The IDEO demonstrated greater posterior strut displacement than traditional AFOs. The IDEO strut deflection can be characterized as column buckling; this deflection mechanism was also observed for the PhatBrace AFO.
   - This finding supports the research hypothesis that the method of strut deflection of the IDEO differs from other AFOs. However, as strut deflection to the full target load was only investigated for three AFO designs; additional testing is required to determine whether the magnitude and deflection mechanism demonstrated by the IDEO are unique.
   - The column buckling deflection mechanism, with peak deflection at the mid-strut level, may contribute to enhanced energy storage/release during gait. Further dynamic testing in needed to investigate energy storage/release.

5. For the IDEO, the ROM of the ankle of the surrogate limb was less than 6.1° for all sub-phases of stance. In addition, the peak force corresponding to 5° ankle dorsiflexion was greatest with the IDEO.

- The IDEO is typically prescribed for patients with fused ankles and/or limited “pain-free” ankle ROM. For the study AFOs, only the IDEO provided sufficient motion constraint for the ankle, confirming its utility for this patient population.
- The increased peak force observed while maintaining limited ankle ROM indicates that the IDEO likely provides greater structural support, protecting the ankle and subtalar joints.
- The thermoplastic solid-ankle and GRF AFOs are also frequently prescribed for the considered patient population. While these AFOs maintained a neutral ankle orientation during MSt, the AFO footplate deformed during TSt and PSw. These alternative AFOs might therefore subject the underlying ankle structure to “painful” rotation.

6. The IDEO demonstrated the greatest rotation of the proximal triad for all stance sub-phases, as well as reduced sagittal plane rotation of the supramalleolar triad.
   - In contrast to the other study AFOs, the increased proximal and reduced distal rotations of the IDEO support the hypothesis that the method of posterior strut deflection for the AFO is unique.
   - The mid-strut buckling induces proximal rotation.
   - The stiff malleolar region and footplate of the IDEO minimize distal rotation, thereby protecting the ankle and subtalar joints.

7. The supramalleolar region of the IDEO demonstrated reduced medial-lateral and superior-inferior motion.
   - The reduced rotation at the supramalleolar region protects the ankle and subtalar joints, as well as the plantar structures of the foot.

- This resistance to frontal and coronal plane deformations facilitate increased load transfer to the more proximal features of the AFO, potentially off-loading the patient's distal shank, ankle and foot.

5.5 Study Limitations

The experimental protocol involving mechanical testing of AFOs with a surrogate limb was designed to characterize the mechanical behavior of various designs. While the study facilitated orthotic loading over the physiologic range during gait, several limitations remain. Modifications to this study are proposed to address the noted limitations.

Mechanical bench testing introduces several limitations that may affect clinical implications. A surrogate limb approximated the human shank and foot. However, this model simplified the joints of the foot and combined the tibia and fibula into a single structure. The surrogate limb was also passive, ignoring the limb musculature. In addition, neural and musculoskeletal pathologies warranting orthotic treatment were not considered. The characterized mechanical properties presented reflect that of the AFO and surrogate limb, not the AFO itself. However, each AFO was tested with the same surrogate limb, facilitating comparison between AFO designs. For the GRF and BlueRocker™ AFOs, the fit of the AFOs was not ideal and the interior surface of the AFO did not have full, intimate contact with surrogate limb, perhaps affecting the results for these two AFOs. The AFO-surrogate limb complex was not shod, potentially affecting the fit of the AFOs and the distribution of load, possibly affecting the results.

The AFOs were tested at discrete loads and orientations to approximate specific instances during the latter sub-phases of stance. The mechanical testing setup might be modified to actuate the loading plate and permit dynamic, continuous testing. Such actuation might incorporate a rack

and pinion setup, similar to Kobayashi et al. [28]. Active markers along the posterior strut and marker triads might again be used to characterize strut deflection and rotation of the AFO during dynamic loading.

Another study limitation was the inability to directly collect moment data to characterize the rotational stiffness of the AFO. Estimation of ankle moment via force and moment arm approximation proved inaccurate due to distributed load along the plantar surface and the changing contact area between the AFO foot plate and the loading plate, and the inaccurate estimation of the effective ankle lever arm. If the aforementioned rack and pinion setup is utilized, ankle moment can be calculated using the radius of the pinion gear and the applied load.

A final limitation of this study was the partial loading of AFOs during compressive stiffness and strut deflection testing. The maximum strut deflection, and perhaps deflection mechanism, is likely dependent on the magnitude of the applied load. Further mechanical testing subjecting each AFO to the full target load is required for a reliable comparison of the compressive stiffness, strut deflection, and deflection mechanisms between all AFO designs.

5.6 Future Work

To further understand the impact AFO designs have on patient gait, particularly during the transition from stance to swing, the energy storage/release of these devices should be evaluated. The results of the current study may provide some insight into energy storage, but additional research is necessary to characterize the mechanism of energy storage/release and quantify AFO energy storage dynamically during gait and other tasks. Energy storage/release should be considered throughout sub-phases of stance, when different characteristics may be desired (i.e. more energy stored during early stance for impact absorption and more energy

release at late stance to aid in transition to swing). Energy release of the AFOs during high energy activities also needs to be characterized. Ankle motion should again be measured during dynamic testing to investigate mechanisms of energy storage/release that protect the ankle and subtalar joints.

Gait analysis might also be conducted, perhaps using able-bodied subjects initially, to investigate the biomechanical function of AFOs. Such analysis might include measurement of posterior strut deflection, AFO deformation, and/or AFO rotation during treadmill ambulation using an active marker motion capture system. Passive markers and motion analysis might be integrated to facilitate simultaneous acquisition of subject joint kinematics. Such testing might confirm study results for the composite AFO-surrogate limb for physiologic limb structures.

The IDEO has been shown to provide improved clinical function over other AFO designs for patients with limb trauma. Enhanced understanding of the mechanics of the IDEO design might provide insight for IDEO re-design for alternative populations and/or new AFO designs. Such studies might manipulate the design features of the IDEO (supramalleolar walls, posterior strut geometry, materials, and stiffness, and footplate stiffness) to direct loading, direct deflection, allow ankle motion, or enhance energy storage/release. Adaptations to the IDEO design for particular patient populations (i.e., a reduced footplate stiffness for formerly active patients with lower limb muscle weakness and an intact ankle structure, or modified posterior strut stiffness for patients sensitive to lower limb loading) may be studied to investigate the functional outcome of these alternative IDEO designs.

CHAPTER 6: CONCLUSIONS

Ankle-foot orthoses (AFOs) are devices used to control and stabilize the lower leg to improve pathological gait due to muscle weakness, spasticity, hypertonicity, instability, and/or chronic pain. Young, formerly-active individuals with traumatic injuries to the lower leg also may rely on AFOs to restrict ankle motion and/or provide assistance at push-off to minimize joint pain during ambulation. Traditionally, AFO designs have been fabricated from thermoplastic materials, but these designs are unable to produce sufficient energy storage and return to facilitate high-intensity activities such as running and jumping. To improve the energy storage and return, as well as to improve durability, carbon fiber composite materials have been incorporated, resulting in thinner, lighter, and stronger designs. One particular carbon graphite and carbon fiber design, the Intrepid Dynamic Exoskeletal Orthosis (IDEO), has demonstrated improved functional performance compared to traditional AFO designs.

To enhance prescription, fitting and alignment, and functional outcomes of AFO designs, it is necessary to understand the biomechanical behavior of the AFO-limb complex during gait. The mechanical properties of an AFO design influence the biomechanical behavioral outcome and can be investigated with mechanical testing. The goal of this study was to develop a mechanical testing method to approximate normal gait and implement this methodology to quantify the compressive stiffness, the deflection of the posterior strut, and the rotation of the proximal and distal segments of the IDEO and other AFOs designs to characterize their mechanical properties.

Each AFO design was donned on a surrogate limb and compressively loaded to simulate the various sub-phases of stance during gait. An inductive ankle angle sensor and motion analysis were used in conjunction with the mechanical testing to quantify ankle rotation, as well as

deflections and rotations of the AFO. While results indicated differences in mechanical properties between the IDEO and traditional AFO designs, the IDEO exhibited a similar final compressive stiffness as the solid-ankle AFO design, suggesting that compressive stiffness alone does not fully characterize mechanical behavior. The IDEO demonstrated greater posterior strut deflection than other AFO designs and the greatest rotation of the proximal segment; the IDEO deflects in a unique, column-bending manner. For the IDEO, the range of motion of the ankle of the internal surrogate limb was less than 6° through all tested sub-phases of stance. In addition, the peak force corresponding to 5° ankle dorsiflexion was greatest with the IDEO. The increased peak force observed while maintaining limited ankle motion indicates that the IDEO likely provides greater structural support, protecting the underlying ankle and subtalar joints.

These results indicate mechanical differences between the IDEO and traditional AFO designs that support the observed clinical differences in function, as well as emphasize the importance of mechanical testing of AFOs. Future work involving gait analysis is needed to confirm these bench top findings. Further studies might also investigate the dynamic energy storage/release mechanisms of AFO designs to improve understanding of the mechanical characteristics and biomechanical function of AFOs.

BIBLIOGRAPHY

[1] P. Bowker, D. N. Condie, B. L. Bader, D. J. Pratt, and W. A. Wallace, eds. *Biomechanical Basis of Orthotic Management*. 1993, Butterworth-Heinemann Ltd: Oxford.

[2] M. M. Lusardi, M. M. Jorge, and C. Nielsen, *Orthotics & prosthetics in rehabilitation*. Third Edition ed. St. Louis, Missouri: Saunders, Elsevier Inc., 2013, pp. 219-239.

[3] S. B. Shawen, J. J. Keeling, J. Branstetter, K. L. Kirk, and J. R. Ficke, "The mangled foot and leg: salvage versus amputation," *Foot and Ankle Clinics*, Vol. 15, pp. 63-75, 2010.

[4] J. J. Keeling, D. E. Gwinn, S. M. Tintle, R. C. Andersen, and F. X. McGuigan, "Short-term outcomes of sever open wartime tibial fractures treated with ring external fixation," *American Journal of Bone and Joint Surgery*, Vol. 90, pp. 2643-2651, 2008.

[5] A. J. Pavlik, "The effect of long-term ankle-foot orthosis use on gait in the poststroke population," *Journal of Prosthetics and Orthotics*, Vol. 20, pp. 49-52, 2008.

[6] E. Cakar, O. Durmus, L. Tekin, U. Dincer, and M. Z. Kiralp, "The ankle-foot orthosis improves balance and reduces fall risk of chronic spastic hemiparetic patients," *European Journal of Physical and Rehabilitation Medicine*, Vol. 46, pp. 363-8, 2010.

[7] Å. Bartonek, M. Eriksson, and E. M. Gutierrez-Farewik, "A new carbon fibre spring orthosis for children with plantarflexor weakness," *Gait & posture*, Vol. 25, pp. 652-656, 2007.

[8] S. I. Wolf, M. Alimusaj, O. Rettig, and L. Doderlein, "Dynamic assist by carbon fiber spring AFOs for patients with myelomeningocele," *Gait & posture*, Vol. 28, pp. 175-177, 2008.

[9] A. Danielsson and K. S. Sunnerhagen, "Energy expenditure in stroke subjects walking with a carbon composite ankle foot orthosis," *Journal of Rehabilitation Medicine*, Vol. 36, pp. 165-168, 2004.

[10] J. C. Patzkowski, R. V. Blanck, J. G. Owens, J. M. Wilken, J. A. Blair, and J. R. Hsu, "Can an ankle-foot orthosis change hearts and minds?," *Journal of Surgical Orthopaedic Advances*, Vol. 20, pp. 8-18, 2010.

[11] J. C. Patzkowski, R. V. Blanck, J. G. Owens, J. M. Wilken, K. L. Kirk, J. C. Wenke, and J. R. Hsu, "Comparative effect of orthosis design on functional performance," *The Journal of Bone and Joint Surgery*, Vol. 94, pp. 507-515, 2012.

[12] J. G. Owens, J. A. Blair, J. C. Patzkowski, R. V. Blanck, and J. R. Hsu, "Return to running and sports participation after limb salvage," *The Journal of Trauma Injury, Infection, and Critical Care*, Vol. 71, pp. 120-124, 2011.

[13] T. Kobayashi, "Techniques to measure rigidity of ankle-foot orthosis: A review," *Journal of Rehabilitation Research & Development*, Vol. 48, pp. 565-576, 2011.

[14] P. Cappa, F. Patane, and M. M. Pierro, "A novel device to evaluate the stiffness of ankle-foot orthosis devices," *Journal of Biomechanical Engineering*, Vol. 125, pp. 913-917, 2003.

[15] L. A. Miller and D. S. Childress, "Analysis of a vertical compliance prosthetic foot," *Journal of Rehabilitation Research & Development*, Vol. 34, pp. 52-57, 1997.

[16] J. Perry, *Gait analysis: normal and pathological function*. Thorofare, NJ: SLACK Inc, 1992.

[17] D. A. Winter, *Biomechanics and Motor Control of Human Gait: Normal, Elderly and Pathological*. Second ed. Waterloo, Ontario: University of Waterloo Press, 1991.

[18] D. A. Nawoczenski and M. E. Epler, *Orthotics in functional rehabilitation of the lower limb*. Philadelphia, PA: W.B. Saunders Company, 1997.

[19] P. M. Nair, K. L. Rooney, S. A. Kautz, and A. L. Behrman, "Stepping with an ankle foot orthosis re-examined: A mechanical perspective for clinical decision making," *Clinical Biomechanics*, Vol. 25, pp. 618-622, 2010.

[20] J. F. Lehmann, P. C. Esselman, M. J. Ko, J. C. Smith, B. J. deLateur, and A. J. Dralle, "Plastic ankle-foot orthoses: evaluation of function," *Archives of Physical Medicine & Rehabilitation*, Vol. 64, pp. 402-7, 1982.

[21] K. Desloovere, G. Molenaers, L. Van Gestel, C. Huenaerts, A. Van Campenhout, B. Callewaert, P. Van de Walle, and J. Seyler, "How can push-off be preserved during use of an ankle foot orthosis in children with hemiplegia? A prospective controlled study," *Gait & posture*, Vol. 24, pp. 142-151, 2006.

[22] N. J. Chladek *Pre-Preg Carbon Dynamic Orthosis*. The O&P EDGE, 2006.

[23] J. C. Patzkowski, J. G. Owens, R. V. Blanck, K. L. Kirk, J. R. Hsu, and t. S. T. R. Consortium, "Deployment after limb salvage for high-energy lower-extremity trauma," *The Journal of Trauma and Acute Care Surgery*, Vol. 73, pp. 112-115, 2012.

[24] E. Russell Esposito, R. V. Blanck, N. G. Harper, J. R. Hsu, and J. M. Wilken, "How does ankle-foot orthosis stiffness affect gait in patients with lower limb salvage?," *Clinical Orthopaedics and Related Research*, Vol. 472, pp. 1-10, 2014.

[25] S. Yamamoto, M. Ebina, M. Iwasaki, S. Kubo, H. Kawai, and T. Kayashi, "Comparative study of mechanical charactersitics of plastic AFOs," *Journal of Prosthetics and Orthotics*, Vol. 5, 1993.

[26] T. Kobayashi, A. K. Leung, and S. W. Hutchins, "Design of a manual device to measure ankle joint stiffness and range of motion," *Prosthetics and orthotics international*, Vol. 35, pp. 478-481, 2011.

[27] T. F. Novacheck, C. Beattie, A. Rozumalski, G. Gent, and G. Kroll, "Quantifying the spring-like properties of ankle-foot orthoses (AFOs)," *Journal of Prosthetics and Orthotics*, Vol. 19, 2007.

[28] T. Kobayashi, A. k. L. Leung, Y. Akazawa, H. Naito, M. Tanaka, and S. W. Hutchins, "Design of an automated device to measure sagittal plane stiffness of an articulated ankle-foot orthosis," *Prosthetics and orthotics international*, Vol. 34, pp. 439-448, 2010.

[29] R. E. Major, P. J. Hewart, and A. M. Macdonald, "A new structural concept in moulded fixed ankle foot orthoses and comparison of the bending stiffness of four constructions," *Prosthetics and orthotics international*, Vol. 28, pp. 44-48, 2004.

[30] M. C. Hawkins, *Experimental and computational analysis of an energy storage composite ankle foot orthosis*, in *Department of Mechnical Engineering*2010, University of Nevada, Las Vegas: UNLV Theses/Dissertations/Professional Papers/Capstones.

[31] R. Singerman, D. J. Hoy, and J. M. Mansour, "Design changes in ankle-foot orthosis intended to alter stiffness also alter orthosis kinematics," *Journal of Prosthetics and Orthotics*, Vol. 11, 1999.

[32] D. J. J. Bregman, A. Rozumalski, D. Koops, V. de Groot, M. Schwartz, and J. Harlaar, "A new method for evaluating ankle foot orthosis characteristics: BRUCE," *Gait & posture*, Vol. 30, pp. 144-149, 2009.

[33] S. I. Ringleb, T. Armstrong, L. J. Berglund, H. B. Kitaoka, and K. R. Kaufman, "Stiffness of the Arizona ankle-foot orthosis before and after modification for gait analysis," *Journal of Prosthetics and Orthotics*, Vol. 21, 2009.

[34] *Draft Report of the American Orthotic and Prosthetic Association Prosthetic Foot Manufacturer Workgroup*, 2009, American Orthotic & Prosthetic Association.

[35] D. Zou, T. He, M. Dailey, K. E. Smith, M. J. Silva, D. R. Sinacore, M. J. Mueller, and M. K. Hastings, "Experimental and computational analysis of composite ankle-foot orthosis," *Journal of Rehabilitation Research & Development*, Vol. 51, pp. 1525-1536, 2014.

[36] I. S. Organization, *ISO 22523:2006(E)*, in *External limb prostheses and external orthoses - Requirements and test methods*2006, ISO: Switzerland.

[37] S. Tenenbaum, S. C. Coleman, and J. W. Brodsky, "Improvement in gait following combined ankle and subtalar arthrodesis," *The Journal of Bone and Joint Surgery*, Vol. 96, pp. 1863-1869, 2014.

[38] S. S. Hiniduma, U. Gamage, and J. Lasenby, "New least squares solutions for estimating the average centre of rotation and the axis of rotation," *Journal of Biomechanics*, Vol. 35, pp. 87-93, 2002.

APPENDIX A: ACRYONYMS AND DEFINITIONS

AFO	Ankle foot orthosis
IDEO	Intrepid Dynamic Exoskeletal Orthosis
ROM	Range of motion
IC	Initial contact
LR	Loading response
MSt	Mid stance
TSt	Terminal stance
PSw	Pre swing
GRF	Ground reaction force

Motion	all movement, translation and/or rotation, in any plane
Displacement	translation in one plane, defined by the global, laboratory-based coordinate system
Deflection	a pattern of movement considering the relationship between multiple markers
Deformation	motion out of the sagittal plane, motion in the frontal and/or transverse planes

APPENDIX B: ANKLE ANGLE SENSOR INFORMATION

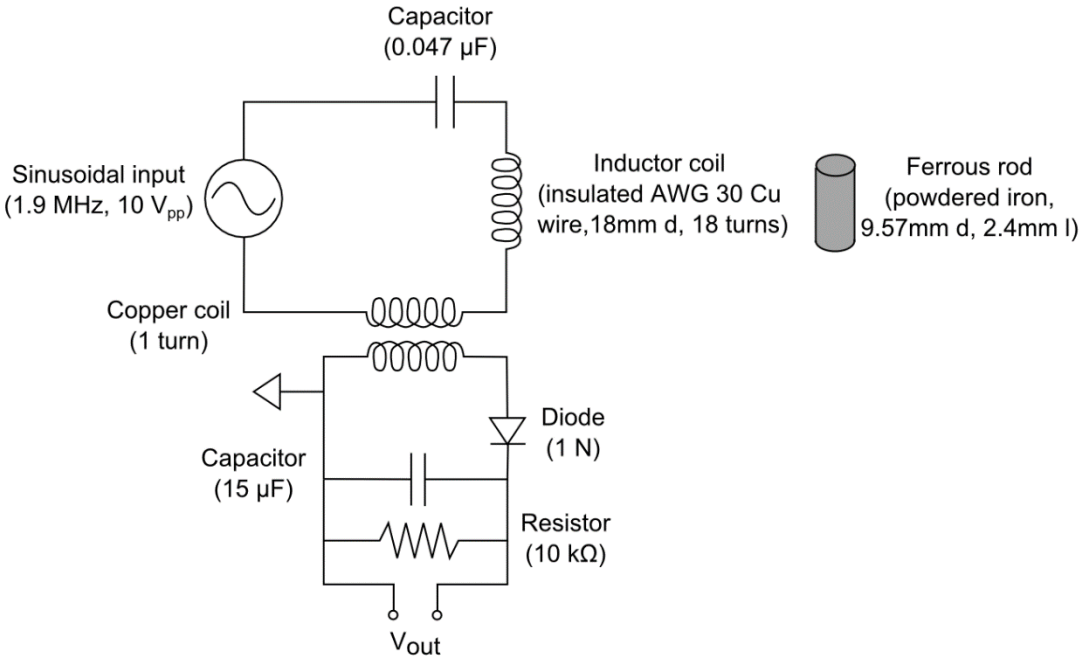

Figure 37: Circuit schematic for inductive ankle angle sensor. Sensor design and function is further described in Section 3.5.1 and Figures 17-19.

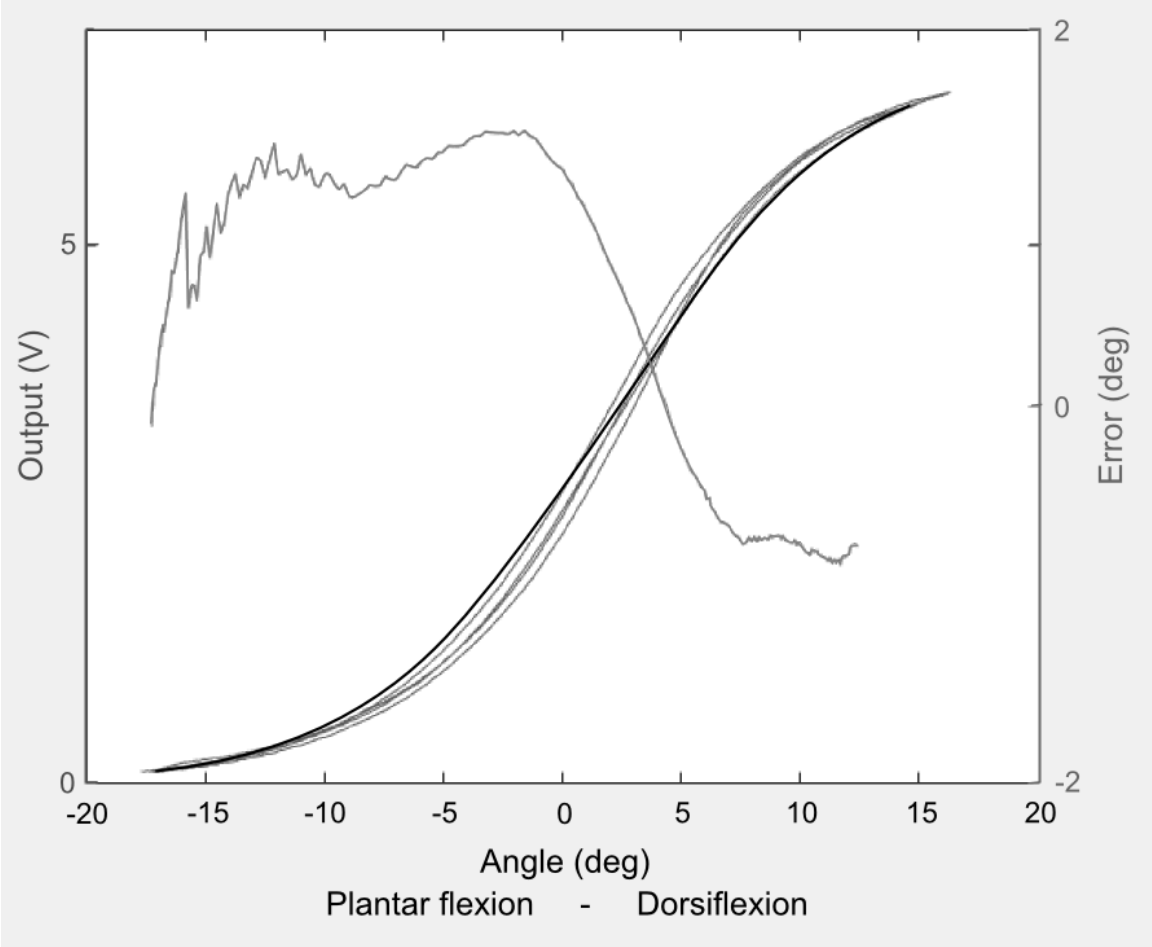

Figure 38: Ankle angle sensor spline calibration curve and corresponding error.

APPENDIX C: PARTIAL LOADING TRIALS RESULTS

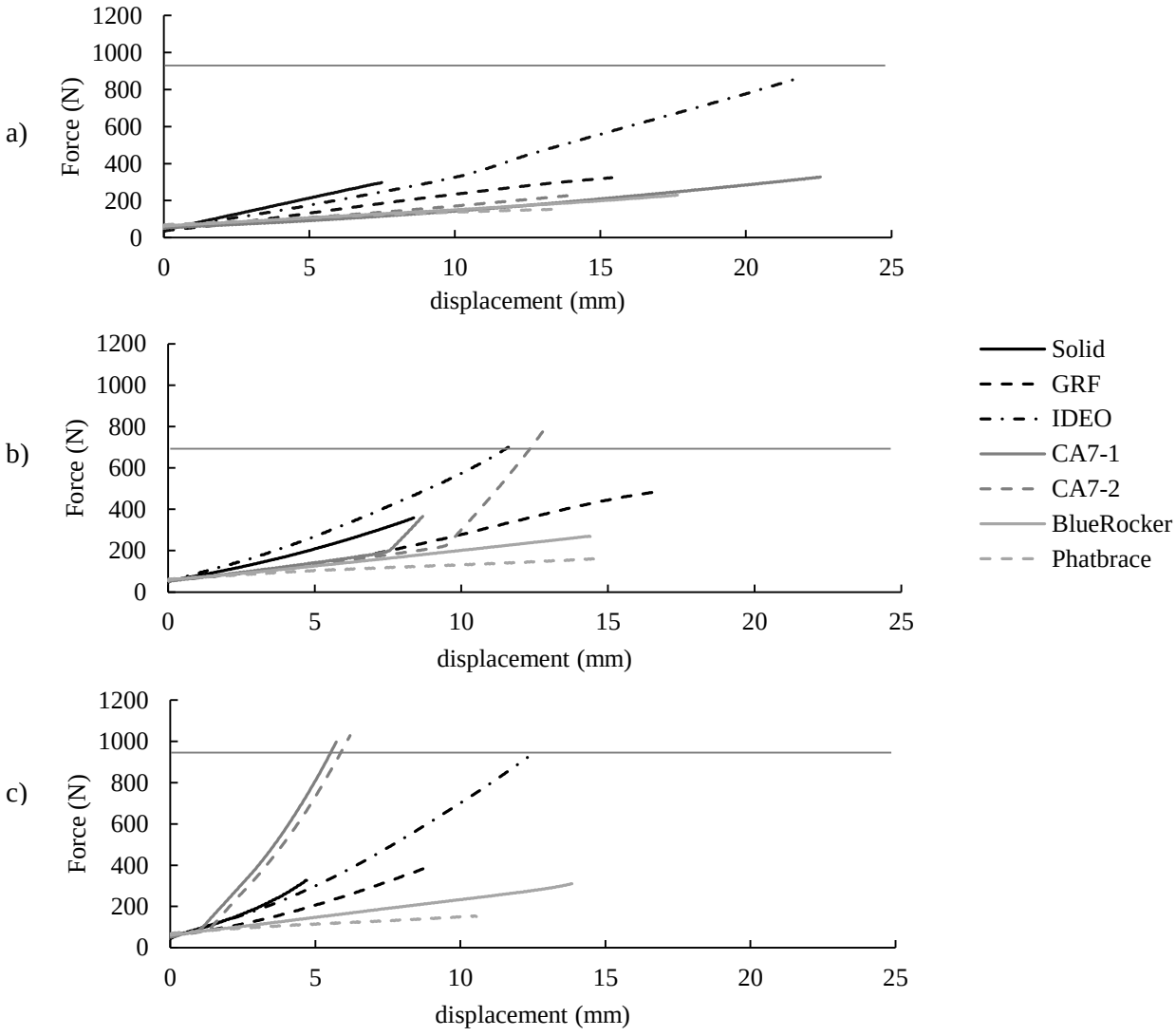

Figure 39: Force-displacement of average loading cycle for each AFO, compressed at 5 mm/s, at each sub-phase of stance: a) MSt, b) TSt, and c) PSw. The target load (solid line) for each phase, 880.7 N for MSt and PSw and 640.5 N for TSt, is noted. Actual final loads are noted in Table 6.

APPENDIX D: LOADING RESPONSE RESULTS

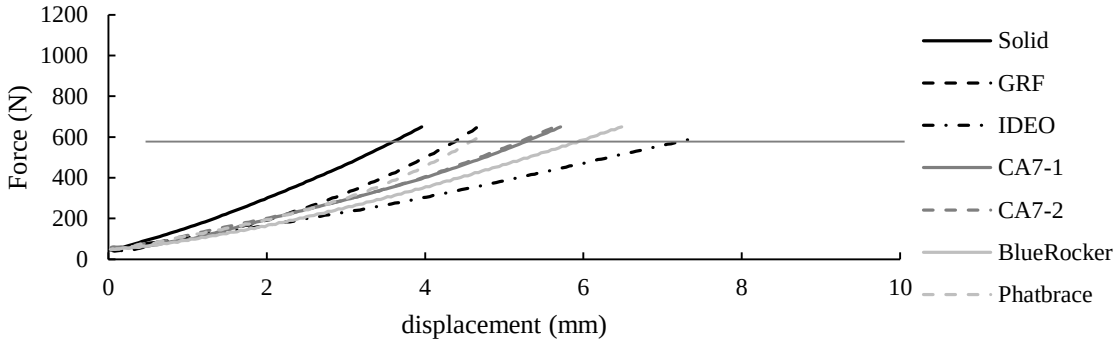

Figure 40: Force-displacement curves for each AFO tested at 5 mm/s during LR conditions. Target load (560.5 N) is noted by the solid horizontal line.

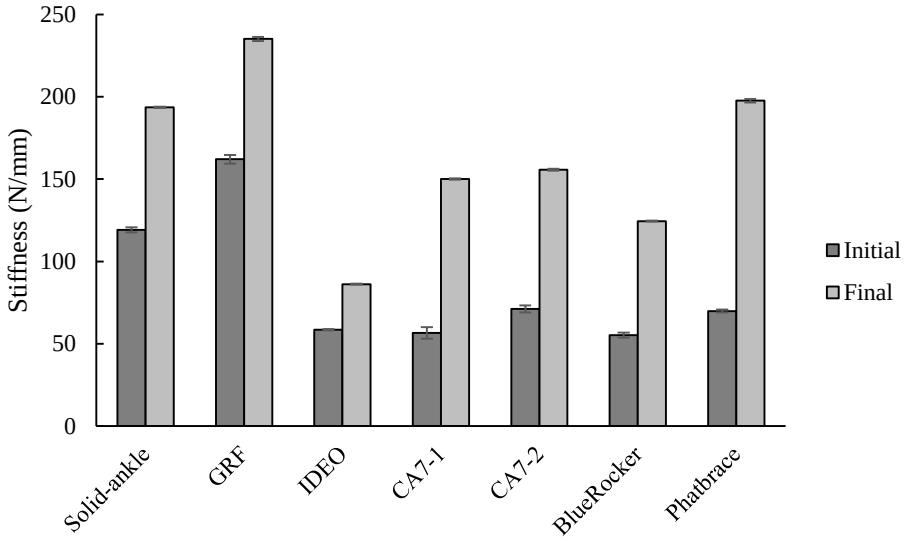

Figure 41: Initial and final compressive stiffness for each AFO tested during LR conditions.

Table 12: Maximum strut displacement in the sagittal plane of each AFO tested at LR conditions.

	Maximum strut deflection (mm)	
	LR	
Solid-ankle	3.53 (± 0.01)	D
GRF	2.65 (± 0.01)	P
IDEO	3.23 (± 0.02)	M
Carbon Ankle 7	4.41 (± 0.03)	D
Carbon Ankle 7 - stiff	4.88 (± 0.03)	D
BlueRocker™	2.63 (± 0.01)	P
PhatBrace	4.79 (± 0.03)	D